



Shahrood University of
Technology



Iranian Society of
Mining Engineering
(IRSM)

Plio-Quaternary Adakite Genesis and Post-collisional Processes: Whole Rock Constraints and Sr, Nd Isotopic Compositions in Alborz Magmatic Belt, Ardabil, Iran

Akram Abdollahadi¹, Seyed Jamal Sheikhzakariaee¹, Abdollah Yazdi^{2*} and Seyed Zahed Mousavi³

1. Department of Geology, Science and Research Branch, Islamic Azad University, Tehran, Iran

2. Department of Geology, Kahnooj Branch, Islamic Azad University, Kahnooj, Iran

3. Department of Geology, Meshkinshahr Branch, Islamic Azad University, Meshkinshahr, Iran

Article Info

Received 13 July 2024

Received in Revised form 30
September 2024

Accepted 21 October 2024

Published online 26 October 2024

DOI: [10.22044/jme.2024.14781.2801](https://doi.org/10.22044/jme.2024.14781.2801)

Keywords

Alborz magmatic belt

Sr-Nd isotopic

Adakite

Sabalan

Iran

Abstract

The Plio-quaternary sub-volcanic domes are the products of magmatism in the Turkish-Iranian plateau in the collision zone between Eurasia and Arabia. Intermediate-felsic volcanic rocks are found 50 km west of Ardabil. These volcanic domes make a significant part of the Sabalan volcanic, a Plio-quaternary stratovolcano in northwest Iran. The igneous rocks (adakitic) include dacite, trachyte, andesite, trachy-andesite, and trachydacite, associated with ignimbrite and pyroclastic equivalents. They mainly comprise phenocrysts and a microcrystalline groundmass of pyroxene, amphibole, and plagioclase, with biotite and titanomagnetite. These rocks are enriched in Light Rare Earth Elements (LRREs) and Large Ion Lithophile Elements (LILEs) and depleted from Heavy Rare Earth Elements (HRREs) and High-Field Strength Elements (HFSEs). In these rocks, the SiO₂ content is 56-66 wt%, Na₂O is > 3.5 wt%, Al₂O₃ > 15 wt%, Yb < 0.2 ppm, and Y < 7 ppm, which are typical of high silica adakitic rocks. The initial ratios of the ¹⁴³Nd/¹⁴⁴Nd range from 0.5127 to 0.5129 and the initial ratios of ⁸⁷Sr/⁸⁶Sr for the adakites range from 0.7035 to 0.7060, reflecting the heterogeneity of the mantle and different degrees of crystallization. These geological, geochemical, and Sr, and Nd isotopic data indicate that these rocks belong to the post-collisional adakite type, and are derived from low-degree partial melting of a subduction-metasomatized continental lithospheric mantle (eclogite or amphibolite garnet). In the studied area, mineralization related to Plio-quaternary adakitic rocks has not been observed.

1. Introduction

Adakitic rocks in the Alpine-Himalayan belt are indicative of the geodynamic evolution of collision zones, and are often associated with mineralization. Recently, adakites have garnered a special attention in Iran as part of a group of arc rocks. Adakites are divided into three categories: 1) Silica is produced due to the partial melting of the mantle wedge 2) High-Si Adakites (HSA) are produced by the partial melting of the subducted oceanic crust [1], and 3) the so-called “continental” adakite (or adakite C), first introduced in eastern China by [2], is formed by the melting of a portion of the garnet-amphibolite lower crust into eclogitic facies. Adakitic rocks have been reported from

northwest, central, and northeast Iran [3-8]. These rocks exhibit high Sr/Y and La/Yb ratios, and have been identified in various geological settings including Supra-Subduction Zones (SSZs), active continental margins, and intra-continental extensional settings [9].

Northwestern Iran is located in a broad zone of continental collision and deformation between the African-Arabian and Eurasian plates. This area has experienced a compressional tectonic regime from the early Cenozoic to the present. In this region, compression has resulted from the subduction of the Neo-Tethysian oceanic crust under the Iranian microplate and the subsequent collision between

✉ Corresponding author: yazdi_mt@yahoo.com (A. Yazdi)

the Arabian and Eurasian plates along the Zagros suture zone [10-12]. The E-W trending Sabalan volcano represents the easternmost Quaternary volcanic belt in the Turkish-Iranian plateau [12]. Its nearest neighbors are the adjacent volcanic chains near the studied area including Sahand (also in NW Iran), Ararat, Tendürek, Süphan, and Nemrut in eastern Anatolia (Turkey), all lying within the Arabia-Eurasia collision zone (Figure 1) [13]. This group of rocks is distributed along the rim of the Van-microplate [14], and is classified into two main groups. The first group includes adakite and adakitic rocks, while the second group comprises high-Nb basaltic rocks [3, 5], indicating that their genesis occurred in a post-collisional tectonic regime. Some major Pliocene-Quaternary volcanoes (e.g. Sahand, Sabalan, and Ararat) erupted during this time [15-17]. Volcanism at Sabalan volcano began around 4.5 to 2.9 Ma, approximately 300 km from the Neo-Tethyan suture zone [17].

2. Regional Geology

In northwestern Iran, Cenozoic activity basically indicates the derivation of magma from mantle sources modified by subduction in both the back-arc tectonic and active collision contexts. Ultrapotassic and adakitic compositions and Pliocene-quaternary-like intraplate magmatic cycles are two witnesses of the contribution of the subduction-modified mantle components [18, 19]. The evidence for the existence of Proto-Tethys, Paleo-Tethys, and Neotethys oceanic basins has been reported from Iran [20-22]. Sabalan volcano is underlain by a low-velocity zone in the lower crust, which is considered thermal in nature [23]. Shahneshin volcano is located 40 km west-southwest of Ardabil, and 25 km southeast of Meshginshahr. According to the provincial divisions of Iran, the mountains of Shahneshin are mainly located in the Ardabil province, although a part of its southwest is located in the east of the Azerbaijan province. The highest peak of this great volcano is called the Sabalan Sultan Mountain. The eruption of domes and viscous magma flows from the fractures inside, and around the caldera on steep slopes has given it a rough morphology [24]. The three important domes of Sabalan are Sultan Savalan volcano, Heram Dagh, and Agham Dagh, which have developed in the northeast-southwest direction. From lithological and morphological perspectives, the Balujeh and Shahneshin Mountain makes a volcanic composite cone

consisting of alternating layers of pyroclasts and lava flows (Figure 1).

Volcanic materials were stacked to form composite cones during various eruption phases and lava flows. The North of Tabriz Fault (NTF) is among the most important strike-slip faults in northwestern Iran. This fault is crucial to the geodynamic pattern of northwest Iran. Along this fault, the seismic history of northwest Iran is centered [25]. A strike-slip displacement precedes an inverted right-hand displacement after the fault. Numerous positive and negative flower structures, and synclines have evolved along this fault. This fault is 120 km long, and stretches from the northwest of Sufiyan to the southeast of Bostan Abad with an N135°E strike [26]. The lithospheric movements, GPS velocity field, shortening rates, and strike-slip movements in northwestern Iran (Figure 1b) suggest that the Sabalan area undergoes an active convergent strike-slip deformation [24]. This deformation was studied more in the west of Sabalan (Figure 1b). According to [24], the Qushadag mountain range acts as a positive flower structure due to its strike-slip deformation. The current maximum stress of this regime was obtained through the inversion method, and focal mechanism of the faults is N125°E, and N132°E, respectively. Since the Quaternary period, non-parallel strike-slip faults, dip-slip faults, and reversal faults have controlled the stress in this area [23]. These authors put forward a conceptual model based on the seismic and geomorphological data. According to this concept, the hard lithosphere of the South Caspian basin governs the kinetic patterns of the active structures in the northeast (i.e. NTF). According to this model, on a regional scale, right-slip faults operate along the NTF, and left-slip faults operate in the NNE direction.

Extensive research works have been conducted on the formation of the Sabalan mountains [27-29]. Transitional (active) transverse faults parallel to orogeny in the Peri-Arabian region have been considered the cause of fissure eruptions and stratovolcanoes in the late Cenozoic including Sabalan (Shahneshin) [30]. The cause of Paleogene magmatism and expansion is explained by the slab rollback or slab retreat phenomena, followed by low slope subsidence during the Cretaceous period. According to the recent research work, local tensile movements in the western region of the Caspian Sea have continued up to the present day, as it expands 4 mm to the northeast and 4 mm to the southwest annually [31].

Sabalan volcano is the product of various tectonic events that occurred in two main orogenic cycles. The first event is the Neothethys within-plate deformation related to the convergence of Arabian-Eurasian plates. The author showed that the Shahneshin (Sabalan) volcano was active on

the continental margin [28]. The second event is the alkaline composition of the rocks in the continental rift, which has a deep magma chamber, and is affected by crustal contamination and assimilation with fractional crystallization (AFC) [32].

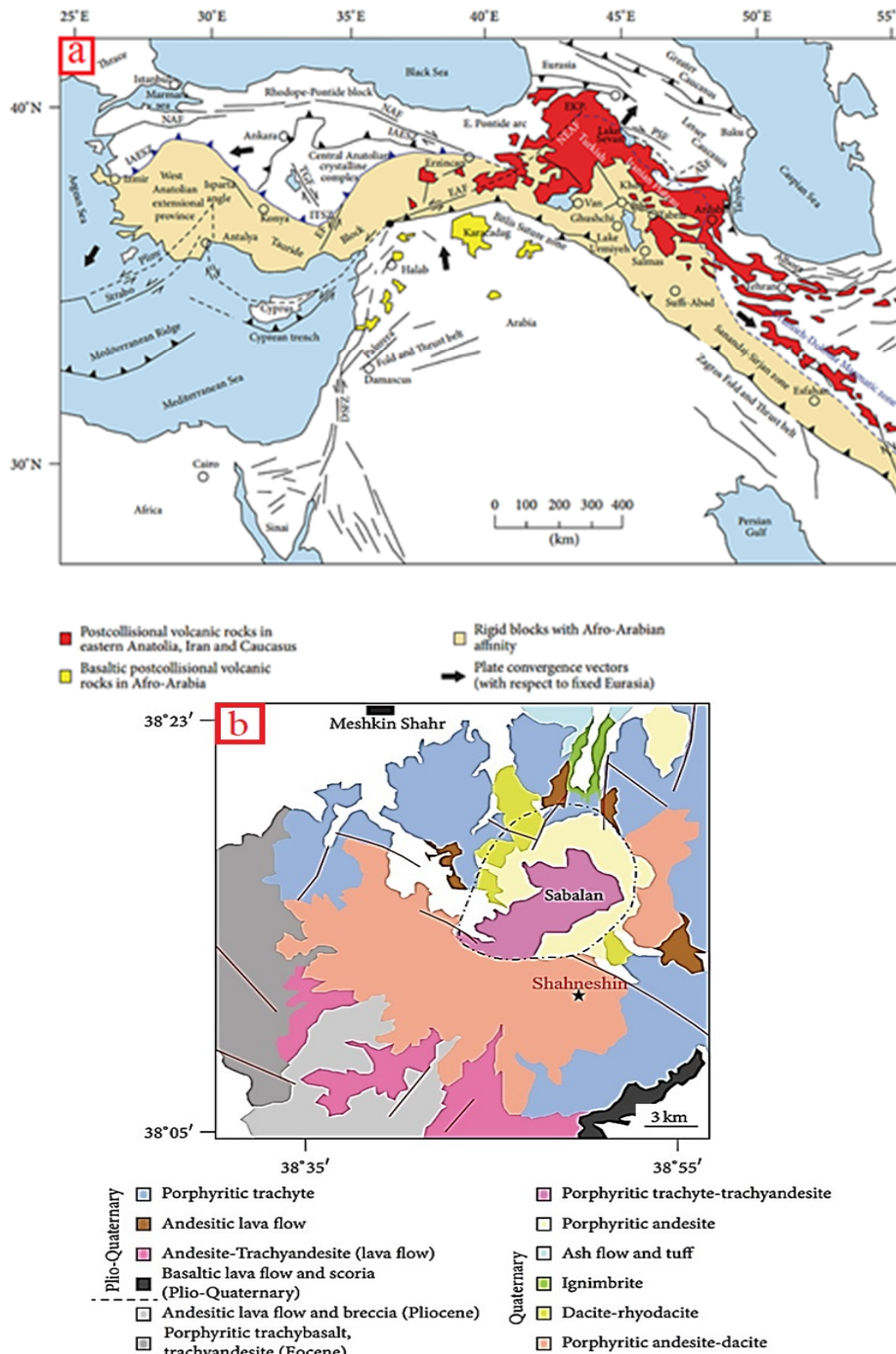


Figure 1. a) Simplified tectonic map of the eastern Mediterranean-Persian Gulf region showing the active plate boundaries and post-collisional volcanic rocks in the Peri-Arabian region modified after [12] (Abbreviation: PSF = Pampak-Sevan fault; EKP = Erzurum-Kars Plateau; EAF = East Anatolian fault; IAESZ = Izmir-Ankara-Erzincan Suture Zone; EF = Ecemis Fault; NAF = North Anatolian Fault; DSFZ = Dead Sea Fault Zone); b) Simplified geological map of the volcano and location of the samples [33].

3. Sampling and Analytical Methods

The samples were collected to evaluate the microscopic, geochemical, and petrogenesis studies in the Shahneshin region. The bulk rock major elements of the samples were analyzed by X-ray fluorescence (XRF) at the Tehran Geological Survey of Iran laboratories. Whole-rock trace elements from the samples of the Shahneshin volcano were analyzed using a Triple Quadrupole Agilent 8800 ICP-MS at the same laboratories. Sample digestion was performed through lithium metaborate fusion.

4. Petrography

Quaternary volcanic rocks of the studied area consist of trachyandesite, andesite, trachy-dacite, and pyroclastic rocks. Under the microscope, basaltic volcanic rocks represent porphyritic, flow, glomeroporphyritic, and sieve textures (Figure 2b). Plagioclases are the most abundant minerals in the rocks of the Shahneshin area.

Plagioclase phenocrysts with one or more mafic minerals (e.g. hornblende and pyroxene) are composed of oligoclase, and andesine (in the Michel-Levy method) exhibit oscillatory zoning, and are often altered to sericite, chlorite, and clay minerals. Secondary quartz is similarly granular in the matrix, and may sometimes fill voids in the rock.

Magnetite and titanomagnetite (opaques) are secondary minerals, while apatite is an accessory mineral in the andesitic rocks of the studied area.

Plagioclase phenocrysts are the most abundant in the dacite-rhyolite lavas. Some crystals exhibit circular and embayment forms with sieve texture and zoning structure. The plagioclase minerals in these rocks have undergone carbonate and sericite alteration. Opacification and corroded margins are additional features of these minerals.

Rhyolite rock matrix often contains alkaline feldspars. Quartz is mostly present in the matrix, and in the micro-phenocrystic form. Quartz has anhedral shapes, and forms isolated interstitial pockets, which appear to have crystallized later than the other minerals. Biotite is euhedral, and partially altered to chlorite.

The andesitic rocks of the area include basaltic andesite, andesite, hornblende-pyroxene andesite, pyroxene andesite, and trachyandesite. These rocks

exhibit a variety of textures including porphyritic, flow, glomeruli-porphyritic, and sieve textures. The rock-forming minerals in these rocks are Plagioclase and one or more mafic minerals such as hornblende and pyroxene (Figure 2c). Plagioclase often crystallizes as zoned phenocrysts with an oligoclase-andesine composition. Plagioclase is altered to sericite, chlorite, and clay minerals in all these rocks. Secondary quartz crystals are also observed as fine grains in the matrix, and, in some cases, as phenocrysts. Other secondary minerals in the andesitic rocks of the area are mostly magnetite, titanomagnetite (opaque minerals), and apatite. Trachyandesites exhibit a porphyritic texture with microlithic and trachytic features and, in some cases, as a mega-porphyritic matrix. The mineralogy of these rocks includes plagioclase crystals and one or more mafic minerals such as hornblende and pyroxene. One of the most prominent features of these rocks is bay-like corrosion at the margins of plagioclase and clinopyroxene, sieve texture in coarse and fine-grained plagioclase, and longitudinal and transverse sections of automorphic hornblende with burned margins. Inclusions of opaque and apatite minerals are observed in these crystals. In some samples, limited occurrences of olivine are also observed (Figures 2a and 2b).

4.1. Crystal lithic lapilli

However, a wide textural difference is observed under the microscope, and its pyroclastic components include crystals and rock fragments. Euhedral to anhedral plagioclases, with fine-grained to medium-grained crystals, are among the most abundant components in the matrix of pyroclastic rocks. Moreover, pyroxenes appear in euhedral to anhedral forms, with micro-crystalline to medium crystal sizes in the pyroclastic rocks. These minerals are often altered from the margins to opaque minerals. The Opaque minerals have a relatively strong rock matrix dispersion, and are subhedral to semi-angular. In the rock matrix, lithics with an average size of 3.5 mm, and a frequency substantially greater than that of crystals may be found. Most of these lithics have andesite and trachyte andesite compositions. The apparent characteristics of these lithics are their semi-angularity and angularity (Figure 2d).

Table 1. Major element (wt%) and trace element (ppm) abundances for rocks of the Shahneshtin volcano.

Sample	SiO ₂	Al ₂ O ₃	Fe ₂ O ₃	FeO	CaO	Na ₂ O	K ₂ O	MgO	TiO ₂	MnO	P ₂ O ₅	LOI
S6-A	66.33	16.16	2.14	1.69	3.68	4.31	2.89	1.51	0.64	0.1	0.42	0.01
20T	66.41	16.1	2.16	1.95	3.65	4.12	2.67	1.68	0.65	0.05	0.43	0.499
43T	62.89	16.96	2.37	2.56	4.35	4.27	3.44	1.61	0.84	0.04	0.55	1.544
S27T	67.67	16.46	2.03	1.17	3.05	4.45	3.09	1.12	0.51	0.07	0.29	1.294
S25T	67.92	16.31	2.02	1.18	3.15	4.29	2.86	1.33	0.51	0.03	0.29	0.795
S29T	69.32	15.22	2.03	1.26	2.94	3.7	3.26	1.28	0.5	0.07	0.34	0.817
38T	66.62	15.81	2.16	1.76	3.83	4.07	2.74	1.71	0.65	0.07	0.44	1.615
42T	68.81	16.15	1.96	0.94	2.91	4.16	2.99	1.24	0.44	0.02	0.26	0.413
S22T	67.26	16.12	2.08	1.37	3.58	4.12	2.68	1.69	0.56	0.06	0.38	0.233
21T	66.56	15.96	2.14	1.64	3.98	4.28	2.57	1.68	0.63	0.05	0.39	1.113
10At	62.37	17.52	2.18	1.84	3.83	4.37	4.8	1.83	0.66	0.07	0.41	1.106
41T	62.98	17.39	2.4	2.59	4.1	4.14	3.59	1.24	0.86	0.07	0.53	0.238
39	68.57	15.74	2.02	1.11	3.18	4.02	2.93	1.48	0.49	0.05	0.32	0.446
S 21	55.8	19.72	2.31	4.17	9.42	4.24	0.36	2.97	0.78	0	0.23	1.843
S 114	62.16	16.87	2.12	2.55	6.95	5.35	1.87	1.38	0.57	0	0.19	1.656
S 49	56.77	18.03	2.29	4.3	8.37	3.66	1.67	3.8	0.71	0.16	0.24	1.5
S 64	59.53	17.04	2.12	4.52	7.82	3.79	1.09	3.14	0.56	0.17	0.21	1
S 66	60.94	19.11	2.17	3.04	7.31	3.74	1.74	1.15	0.63	0	0.16	0.65
S 129	63.71	15.35	1.91	2.4	7.12	4.66	1.64	2.55	0.38	0.1	0.16	0.66
S 131	58.19	20.08	2.2	3.75	7.99	4.39	1.4	1.1	0.67	0	0.22	0.95
S33	60.66	18.32	2.2	2.91	7.09	4.36	1.88	1.71	0.65	0	0.22	1

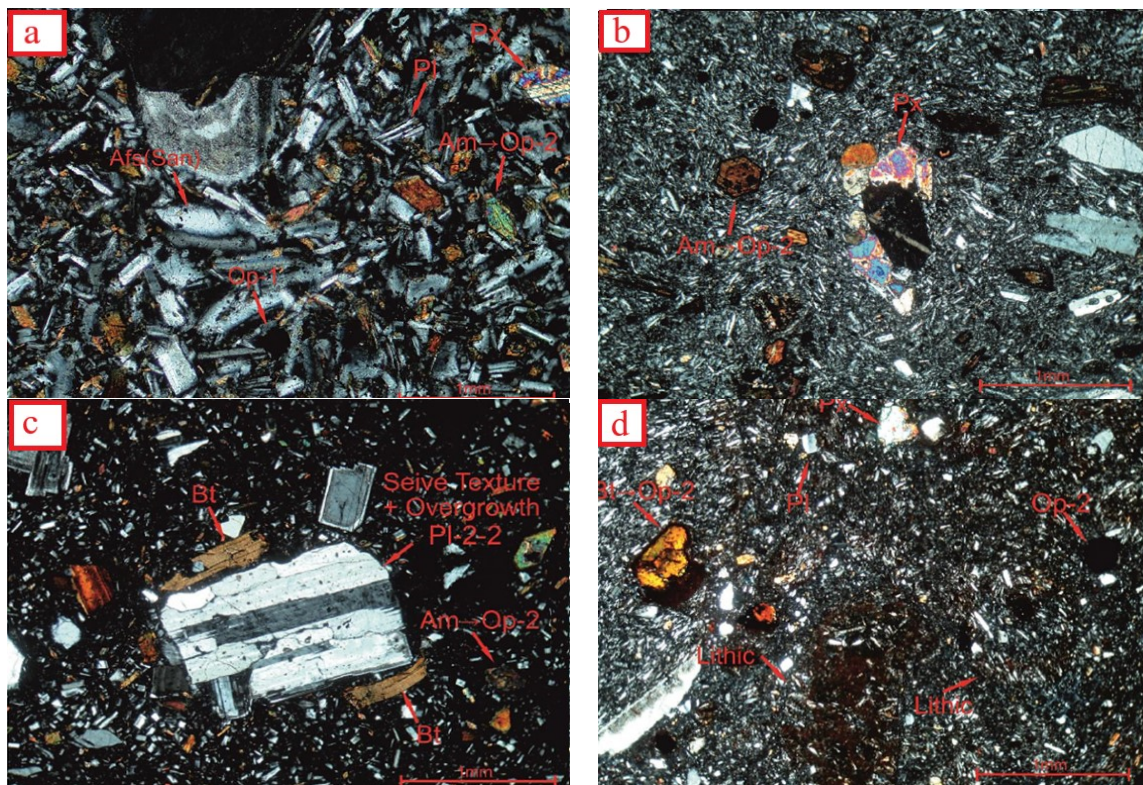


Figure 2. a) A view of amphibole and pyroxene micro-crystals with dual twin (Plagioclase and alkali feldspar type of sanidine) and opaque mineral forming a matrix in trachyandesite; b) a view of euhedral amphibole phenocrysts and aggregate pyroxene in the basaltic andesite matrix; c) a view of plagioclase phenocrysts with an unbalanced sieve texture in the outer margin of the mineral along with growth and blade biotites in the trachy-andesite; d) another view of plagioclase, pyroxene, and flaky biotite crystals converted to opaque minerals and angular andesitic lithics (Abbreviations: Kfs = K-feldspar, Pl = plagioclase, Bt = biotite, Qz = quartz, Cpx = clinopyroxene, and Hbl = hornblende).

Table 2. Trace element (ppm) abundances for rocks of the Shahneshtin volcano.

EL	S6-A	20T	43T	S27T	S25T	S29T	38T	42T	S22T	21T	10-AT	41T	39	S 21	S 114	S 49	S 64	S 66	S 129	S 131	S33
Ag	0.26	0.56	0.36	1.39	0.23	0.22	0.36	0.22	0.26	0.24	0.25	1.27	0.16	0.07	0.13	0.18	0.18	0.29	0.16	0.22	0.21
As	8	5	6	7	6	6	5	10	8	9	7	8	3	2	2.7	8.1	1.8	4.2	6.1	6	4.7
Ba	717.4	719	720.8	665	681.2	666.9	745.2	705	669.5	688.6	716.7	780	684.1	140	374	1738	458	446	534	442	380
Be	1.67	1.58	2.14	1.88	1.75	1.8	1.51	1.69	1.58	1.37	1.5	1.98	1.79	0.5	1	1.2	0.9	1	1.2	1	0.9
Bi	0.07	0.07	0.08	0.05	0.04	0.09	0.07	0.03	0.04	0.04	0.03	0.06	0.03	0.09	0.02	0.04	0.02	0.02	0.02	0.05	0.02
Cd	0.8	0.99	0.58	0.4	1.05	0.09	0.53	0.6	0.19	0.9	1.38	0.82	0.01	0.05	0.04	0.04	0.08	0.05	0.02	0.01	0.01
Ce	90.48	91.1	110.1	73.7	72.92	79.61	84.4	69.7	76.01	82.02	86.42	102.2	72.87	12.3	29.9	48.5	23.4	24.1	40	21.9	27.5
Co	0.99	0.39	0.36	0.95	0.24	1.07	1.26	0.84	1.42	1.44	1.56	0.06	1.92	30.5	13.5	19.3	17.5	16.4	13.3	17.9	13.9
Cr	38	32	16	44	44	38	43	49	27	36	40	29	50	128	60.5	45.8	37.4	42.1	51.8	73.7	50.3
Cs	0.09	0.03	1.25	2.84	1.08	1.71	0.07	1.37	0.59	0.04	0.03	0.79	0.04	0.2	1.86	2.94	1.12	2.06	2.64	1.49	1.72
Cu	32.5	31.9	45.4	50.4	10.3	23.7	33.5	11.8	15.3	32.3	27.3	53.2	10.8	79.5	34.3	52.1	64.7	51.8	41.7	57.6	24.5
Dy	1.46	1.4	1.54	0.82	0.86	0.89	0.93	0.52	0.8	0.73	0.75	1.26	0.73	3.03	2.1	2.44	2.98	2.12	1.74	1.75	1.38
Er	0.75	0.73	1.19	0.7	0.61	0.58	0.62	0.45	0.64	0.6	0.65	1.16	0.48	1.63	1.14	1.4	1.77	1.22	0.99	0.98	0.81
Eu	1.99	1.89	2.18	1.58	1.54	1.57	1.73	1.47	1.58	1.74	1.83	2.15	1.16	0.96	0.83	1.32	0.99	0.85	0.92	0.82	0.64
Gd	3.78	3.63	4.4	3.08	2.77	2.88	3.23	2.5	2.93	3.17	3.41	4.26	2.1	3.04	2.51	3.34	3.16	2.43	2.34	2.02	1.77
Hf	2.35	2.37	4.73	2.05	2.23	1.93	2.22	1.84	2.48	2.02	2.18	4.17	0.2	1.89	2.55	2.71	3.1	3.05	3.02	2.07	1.72
Ho	0.18	0.19	0.36	0.15	0.13	0.14	0.14	0.16	0.21	0.22	0.15	0.33	0.11	0.55	0.37	0.43	0.55	0.39	0.33	0.32	0.25
In	0.22	0.24	0.22	0.23	0.22	0.22	0.21	0.26	0.26	0.22	0.21	0.22	0.22	0.05	0.02	0.04	0.05	0.03	0.03	0.04	0.03
La	50.04	50.4	58.48	39.9	39.93	41.52	48.14	38.7	40.44	44.76	49.18	57.99	39.08	5.4	15.2	26.4	10.4	11.7	21.4	10.6	14.9
Li	7	8	7	6	8	10	10	11	11	7	9	10	8	6.1	18.8	13.6	16.2	6.5	21.8	9.3	7.7
Lu	0.08	0.08	0.16	0.08	0.07	0.07	0.07	0.05	0.07	0.06	0.07	0.15	0.02	0.22	0.17	0.2	0.28	0.18	0.14	0.13	0.11
Mn	512	519	430	445	468	462	522	386	489	459	500	379	466	1110	696	910	1004	712	602	722	592
Mo	3.05	1.98	1.11	0.88	1.06	3.82	0.13	4.53	0.96	0.55	0.69	0.64	0.25	0.72	1.45	1.63	0.89	1.14	1.76	1.05	1.2
Nb	8.8	10.4	28.2	8.55	2.11	9.3	7.45	11.3	10.05	3.52	6.05	18.35	0.07	5.4	7.2	7.7	6.1	6.9	5.9	4.1	4.1
Nd	17.81	15.8	44.8	6	5.03	5.11	10.68	4.49	5.52	9.51	13.44	39.54	8.15	7.7	12	19.5	12.1	11	15	10.6	10.9
Ni	16	16	30	10	9	10	18	21	14	11	14	32	16	72.3	31.2	23.9	13.9	23.7	21.8	24.8	26.9
Pb	11.97	11.8	10.76	17.1	14.85	10.35	8.37	13.7	7.54	8.53	9.08	15.95	18.46	3	9	16	7	10	15	9	10
Rb	51.2	48	108	83.3	68.7	79.2	38	71.9	60.2	37.6	43.6	104	5.6	5.5	33.7	43.3	23.5	36.1	43.4	24.5	30.6
S	95	133	267	103	125	77	116	157	98	75	94	140	119	0.23	0.43	0.57	0.28	0.51	0.69	0.42	0.43
Sb	5.14	1.31	5.28	8.76	4.47	0.94	0.17	3.95	8.56	6.51	17.99	0.22	0.09	22.7	10.1	13.6	12.4	12.8	9.3	9.4	8
Sc	5.9	5.9	8.7	4.6	4.7	4.7	6	3.8	4.8	5.7	5.5	8.5	4.2	2	2	2	2	2	2	2	2
Sm	6.04	5.77	7.09	4.68	4.42	4.56	5.23	4.1	4.6	5.09	5.41	6.75	4.15	2.45	2.46	3.71	2.87	2.35	2.87	2.33	2.01
Sn	0.06	0.07	0.07	0.12	0.05	0.06	0.13	0.1	0.1	0.05	0.06	0.06	0.04	3	3	3	3	3	3	3	3
Sr	1032	1035	915.3	737	788.1	793.4	1047.1	798	825.6	1047	1024	927.5	747.7	298	546	3237	905	967	814	945	613
Ta	1.12	1.16	2.45	1.1	0.91	1.43	1.01	1.44	1.42	0.91	1.09	1.98	0.09	0.87	0.52	0.75	0.49	0.65	2.53	1.46	0.96
Tb	0.39	0.35	0.55	0.29	0.25	0.26	0.32	0.2	0.27	0.3	0.33	0.53	0.23	0.48	0.35	0.43	0.48	0.35	0.34	0.3	0.24
Tc	1.38	1.38	1.37	1.41	1.4	1.4	1.43	1.42	1.43	1.42	1.39	1.37	1.8	0.05	0.05	0.05	0.05	0.05	0.08	0.05	0.05
Th	12.54	12.2	25.3	14.4	13.46	16.33	10.51	15	12.08	10.43	11.33	23.58	0.14	1	4.8	8.4	2.2	2.9	7.2	1.6	3.6
Tl	0.08	0.1	0.16	0.41	0.22	0.28	0.09	0.26	0.22	0.03	0.09	0.16	0.03	0.03	0.12	0.19	0.12	0.17	0.35	0.14	0.17
Tm	0.12	0.1	0.17	0.09	0.09	0.12	0.1	0.08	0.08	0.16	0.12	0.21	0.05	0.23	0.18	0.2	0.26	0.18	0.15	0.15	0.12
U	3.52	3.37	6.71	4.21	3.8	4.65	2.68	4.25	3.51	2.77	3.27	6.5	0.49	0.2	1.2	2.8	0.5	0.8	1.8	0.6	1
V	68	69	92	48	52	52	58	45	55	52	68	87	48	184	85.9	141	103	126	79.1	127	90.1
W	0.38	0.48	1.83	0.61	0.43	1	0.17	1.06	0.74	0.07	0.32	1.88	0.18	0.3	0.8	1.3	0.5	0.7	1.4	0.7	1
Y	9.9	9.7	15.2	10.7	9.4	7.9	10	7.3	9.1	9	9.4	15.8	9.3	15.3	10.8	13	15.6	10.9	9.5	8.8	7.1
Yb	0.2	0.19	0.87	0.18	0.12	0.19	0.25	0.15	0.19	0.34	0.35	0.79	0.25	1.5	1.1	1.3	1.7	1.1	0.9	0.9	0.7
Zn	71.9	74	80.7	67	65.2	60.9	71.3	56.3	58.6	80.5	70.5	89.9	59.9	92.4	58	74	73.1	69.9	66	71.9	57.8

5. Geochemistry

Different petrological processes such as differential crystallization, magmatic mixing, pollution, or a combination of these can be

investigated through geochemical studies. The distribution and dispersion of various elements in the rock units of each region, as well as the relationships and dependencies among these elements, are among the most important aspects

considered in geochemical studies. These relationships shed light on the environment and processes involved in producing rocks. The analysis of rocks' major and trace components in the studied area is shown in Table 1. In the diagram [34, 35], the studied rocks are located in the

combined boundaries of andesite, trachyandesite, rhyodacite, dacite, and trachydacite. The samples from the studied area fall within the sub-alkaline range [36]. In the K_2O - SiO_2 bivariate diagram [37] (Figure 3d), the studied rocks plot in the high-K calc-alkaline series.

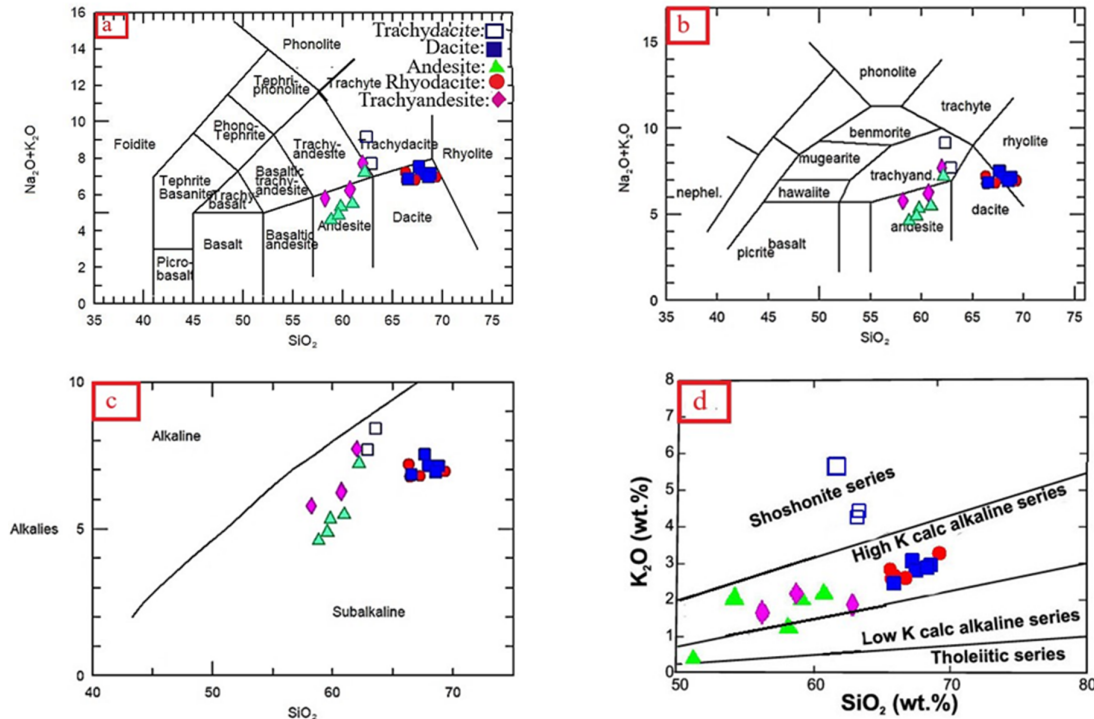


Figure 3. a) Diagram SiO_2 vs. $Na_2O + K_2O$ of [34], b) diagram SiO_2 vs. $Na_2O + K_2O$ of [35], c) diagram SiO_2 vs. $Na_2O + K_2O$ of [36], d) diagram SiO_2 vs. K_2O of [37].

5.1. Crystallization or continental contamination

The chemical effects of different processes including differential crystallization, magmatic mixing, contamination, or a combination of them can be identified through geochemical studies. The distribution and dispersion of different elements in the rock units of each region and the relationships and dependencies among these elements are among the most important aspects considered in the geochemical studies. These relationships shed light on the environment and processes involved in the formation of rocks. Figure 4 presents the diagram of the main elements' oxide variation against SiO_2 (Harker diagram). Among these oxides, the MgO concentration decreases with the increase in the silica concentration. However, the scattering of this data is attributed to Na mobility, caused by alteration and crustal contamination. The range of changes in Al_2O_3 varies from 14.12 wt% in pyroxene andesites to 21.14 wt% in rhyodacite.

The trend of Al_2O_3 versus SiO_2 is descending, which seems normal in terms of the presence of Ca and Al -rich Plagioclase in the basaltic to intermediate rocks. However, some observed scatterings are also related to the number of plagioclase phenocrysts. In contrast, the trends of CaO , MgO , and TiO_2 against SiO_2 are regular and descending. This trend can be explained by the crystallization and reduction of mafic minerals, opaques, and calcium-containing plagioclase. The trend of K_2O versus SiO_2 is ascending due to crystallization, and is less dispersed than Na_2O (Figure 4).

Since all Shahneshin rocks have a low MgO (3 wt%), direct derivation via partial melting of peridotite-mantle parental magma can be ruled out. Based on systematic variations of major elements (Figure 4), with increasing SiO_2 , Na_2O , Al_2O_3 , and K_2O and decreasing TiO_2 , MgO , P_2O_5 , Fe_2O_3 , and CaO , fractional crystallization is identified as a major factor controlling the compositional diversity.

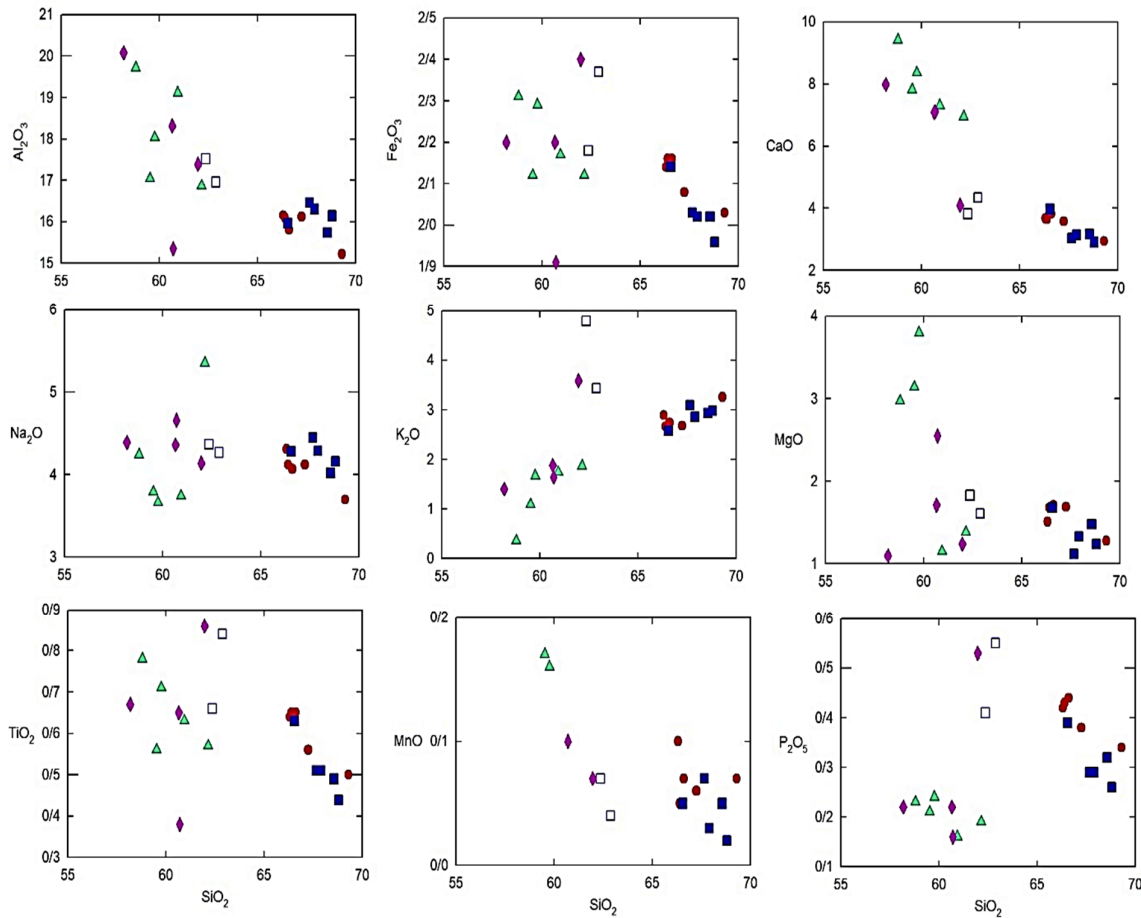


Figure 4. Diagrams of changes of the main elements against SiO_2 .

The distribution diagrams indicate the trace element and REE distribution for the rocks in the studied area normalized to the primitive mantle and OIB values.

Figures 5a and 5b illustrate the chondrite-normalized diagrams of Rare Earth Elements (REEs) for the samples in the studied area [38]. These diagrams show no specific anomaly in Eu, probably due to the lack of subtraction of plagioclase and clinopyroxene during the evolution of the magma forming the rocks of the studied area [2]. The presence of relatively high amounts of Al_2O_3 in the region's rocks (with an average of 17.95 wt%) confirms the absence of plagioclase in the residual phases. However, the Eu separation coefficients between plagioclase and basalt melt are low when oxygen activity is high, and this element behaves as Eu^{+3} along with REEs [39, 40]. In a chondrite-normalized REE plot, parallel patterns with high LREE/HREE ratios are observed. Considering high separation coefficients for HREEs by garnet, this mineral can affect the distribution pattern of elements. The Sr, Rb, Nb, Pb, and Ba levels exhibit some positive and

negative anomalies in the main primitive mantle-normalized diagram (Figures 5a and 5b).

Ti and P are High-Field Strength Elements (HFSEs) that do not move about during the secondary processes. Hence, it is possible to analyze their anomalies using petrological considerations. For instance, Yb is a compatible element in the garnet composition, while La is incompatible. Therefore, the La/Yb ratio varies sharply at low melting points in the source mantle [41]. HREEs are compatible with garnet [42], whereas Medium Rare Earth Elements (MREEs) behave inconsistently. Additionally, at pressures between 3 and 6 GPa, garnet can remain in the source only at very low degrees of melting. Thus, as shown in Figures 5a and 5b, the 10-times enrichment of LREEs compared with HREEs in most of the studied samples suggest the presence of garnet in the mantle source. Negative anomalies in Nb also indicate that magmatic contamination of the continental crust played an important role in the development of the studied area rock. A significant Sr anomaly reveals the existence of plagioclase phenocrysts in the rocks. Meanwhile, very positive

Pb and Ba anomalies suggest a continental crustal contamination. The lack of distinct Ce or Eu anomalies (some even exhibiting weakly positive Eu anomalies) indicates plagioclase fractionation. In the chondrite-normalized REE and primitive mantle-normalized multi-element plots [38] (Figure 5), the region's rocks generally exhibit

similar arc-type patterns. These patterns include LREE enrichments (between EMORB and OIB), HREE depletions (relative to MORB), negative Nb-Ta-Ti anomalies, and positive Pb-Sr anomalies. According to these observations, it is inferred that both rock suites have formed in a subduction-related setting.

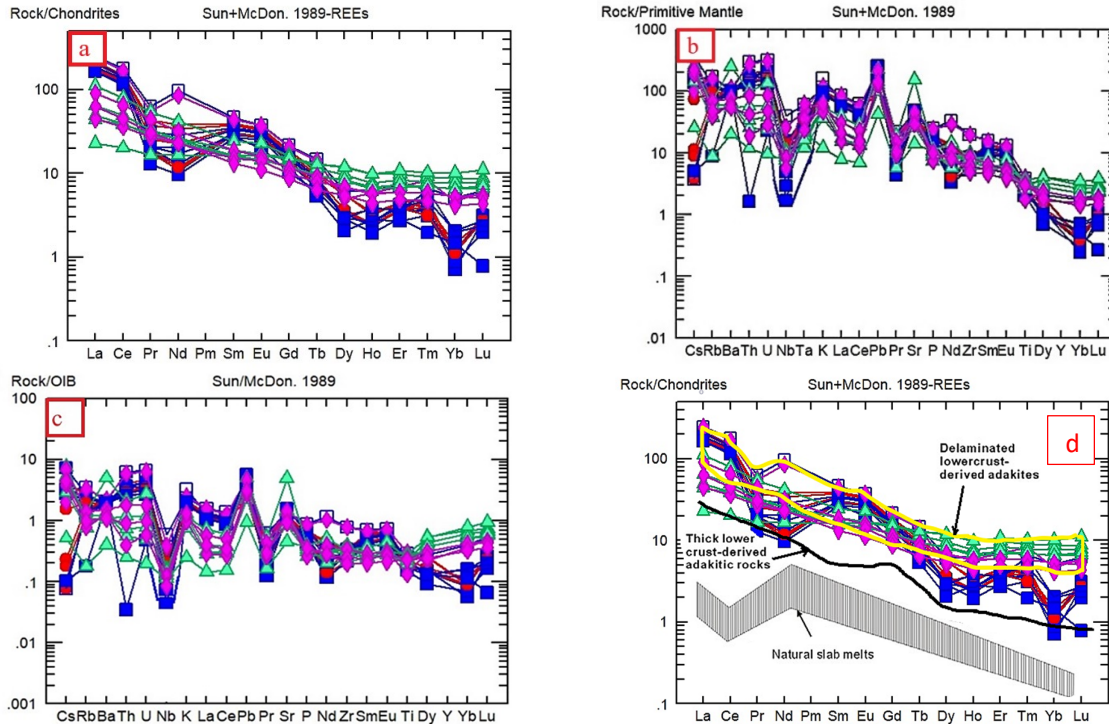


Figure 5. a) Chondrite-normalized REE plot for the rocks of the studied area; b) and c) primitive mantle normalized trace element patterns and OIB for rocks of the studied area [38]; d) the REE and trace element data for delaminated lower crust-derived adakitic rocks, subducted oceanic crust-derived adakites, and thick lower crust-derived adakites and natural slab melts [43, 44].

High Ba content, low Rb/Sr ratio, and high ratios of Sr/Y and La/Yb are characteristics of the studied area rocks. The diagrams of these rocks in the adakite field in the Sr/Y versus Y and La/Yb versus Yb are presented in Figures 6a and 6b. These plots resemble those of typical adakites, as defined in [45].

The low abundances of HREE and Ti in the rocks of the studied area may be related to the stability of amphibole and rutile in the magma source or magma reservoir. Zr is mainly concentrated in zircon, amphibole, and garnet in high-grade metamorphic rocks, with amphibole hosting a higher Zr content compared with that of garnet [46]. The low contents of TiO₂, Sm, and Zr and high Na/Ta in the rocks of the studied area, and the lack of negative Lu and Yb anomalies support the main role of amphibole in the evolution of melts. The Dy/Yb and La/Yb versus SiO₂ (wt%)

diagram [47] shows decreasing Dy/Yb and increasing La/Yb with SiO₂, which are consistent with amphibole control for these magmas (Figures 7a and 7b).

6. Nature of Adakite Rocks

Specific geochemical criteria are used to define adakites or adakite rocks. These criteria mainly include high Sr (≥ 400 ppm), low Y (≤ 18 ppm), low Yb (≤ 1.9 ppm), high Sr/Y (≥ 20), and high La/Yb (≥ 20). Also Mg# (= 0.5), Rb (≤ 65 ppm), K₂O/Na₂O (= 0.42), and SiO₂ (≤ 52 wt%) are the other chemical criteria defined for adakites [45, 49, 50, 54].

These rocks are often the products of partial melting of the oceanic crust, and are found in many continental or oceanic volcanic arcs [55-56]. In the recent years, thorough geochemical analyses of igneous rocks in Iran have allowed for the discovery and reporting of these rocks in various

regions [55]. In northwestern Iran (in the Tabriz-Hamadan volcanic zone), there are adakite dacite

domes with high Sr and Sr/Y ratios and low Nb, Ti, and Y [57].

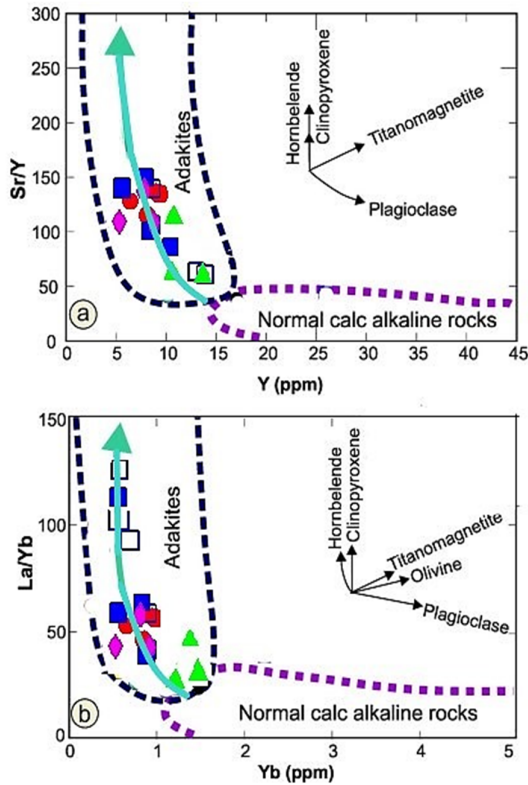


Figure 6. a) Sr/Y versus Y and b) La/Yb versus Yb diagram for rocks of the Shahneshin volcano; these rocks plot in the adakite field in the Sr/Y versus Y and La/Yb versus Yb diagrams [45]. The distribution of the samples around the green arrow line confirms the important role of hornblende in controlling magmatic differentiation [49].

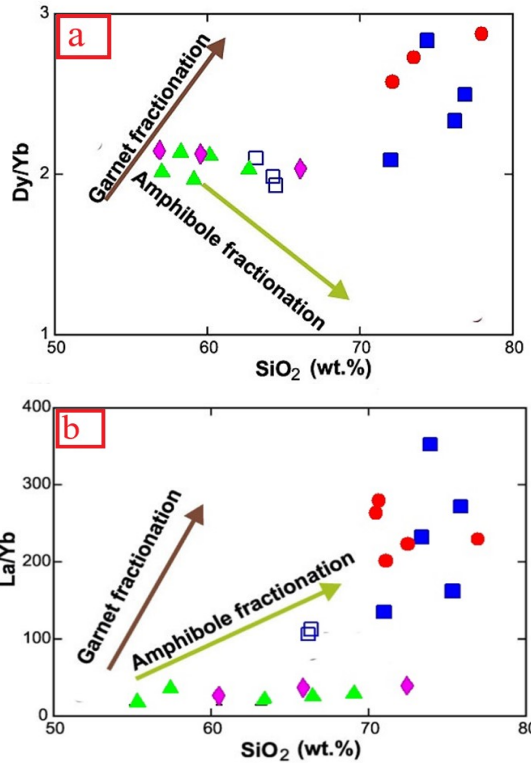


Figure 7. Variation of Dy/Yb and La/Yb ratios versus SiO₂ (wt%), showing decreasing Dy/Yb ratios and increasing La/Yb ratios (a, b), which are more consistent with fractionation controlled by amphibole rather than garnet. Garnet, and amphibole trends from [47].

Table 3. Comparison of chemical properties of the Shahneshin rocks with the properties introduced for adakites.

Elements	Min.	max	Ave.	Adakites
SiO ₂	62.98	69.32	66.59	≥ 56
Al ₂ O ₃	15.74	17.52	16.30	≥ 15
Na ₂ O	3.70	4.45	4.18	≥ 3.5
K ₂ O	2.57	3.59	2.96	≤ 3
MgO	1.24	1.83	1.49	≤ 3
Ni	11.00	30.00	16.69	≥ 20
Rb	5.60	108.00	61.48	≤ 65
Sr	747.70	1035.30	901.42	≥ 400
Y	7.30	1035.30	88.63	≤ 18
Yb	0.20	0.79	0.31	≤ 1.9
Cr	16.00	50.00	37.38	≥ 30
La/Yb	73.41	332.75	193.92	≥ 20
K ₂ O/Na ₂ O	0.69	0.81	0.71	~0.42
Sr/Y	102.42	1.00	87.36	≥ 20
Mg#	24.85	49.05	40.47	~0.5

In terms of the chemical composition of major oxides (e.g. Al_2O_3 , K_2O , Na_2O , MgO , SiO_2 , $\text{K}_2\text{O}/\text{Na}_2\text{O}$, and $\text{Mg}\#$), and REES (e.g. Cr, Ni, Yb, Y, Sr, and Rb), and La/Yb and Sr/Y ratios, the studied dacites lie within the range of the adakitic rocks. Moreover, considering the SiO_2 concentration in the region's rocks (66-62 wt%), these rocks are consistent with high-silica adakites (Figures 8a and 8b). This outcome is explained by the high HREE depletion in adakitic melt.

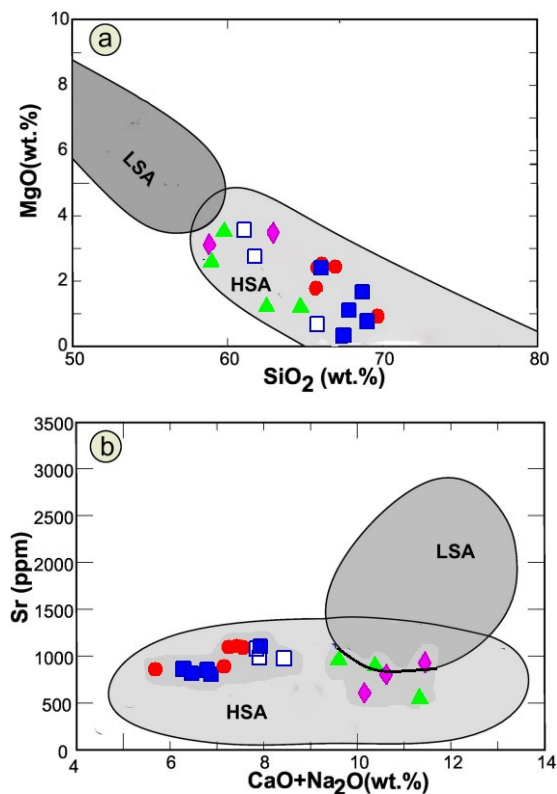


Figure 8. a) and b) Chemical classification for Low-Silica Adakites (LSAs) and High-Silica Adakites (HSAs) [53].

The chemical characteristics of adakites from the subducted oceanic slab are attributed to the melting of an eclogite or amphibolite source [45]. For instance, the high Sr concentration is due to the absence of Sr in the unmelted residue or the lack of differential plagioclase crystallization. Meanwhile, the low Y concentration is attributed to garnet, hornblende, and clinopyroxene. In other words, adakitic melts may be created by dehydrating an amphibolite source or partially melting a basaltic

magma under the garnet stability conditions (eclogite facies) [53-58]. When the predominant mineralogical phase is at the garnet source, the Y/Yb ratio of the adakitic melt is usually greater than 10 [59]. The average of the Y/Yb ratio in the studied area samples is about 17 ppm. According to Figure 9a and the mentioned points, the Adakitic magma forming the rocks in the studied area was produced by the melting of amphibolite and garnet amphibolite oceanic crust (Figures 9a and 9b) through a low degree of partial melting (< 10%) (Figure 9c). Because the Shahneshin lavas are characterized by a higher La/Sm ratio, their mantle source may contain a more modal garnet content than the model source in Figures 7c and 7d, and/or contain other minor phases, the same as phlogopite.

The presence of rutile in the metamorphosed slab and the dehydration of a subducting slab cause rutile to selectively deplete coexisting fluids in HFSEs relative to large ion lithophile elements (LILEs). In the suprasubduction zones, LILEs (Sr, Ba, and Pb) are subduction-mobile elements. Here, migration of Sr, Ba, and Pb-enriched fluids to the mantle wedge can directly trigger partial melting, and generate magmas with elevated Ba/Th, Sr/Th, and U/Th ratios [60]. Due to the fluid released from the subducting slab, a higher degree of melting is common in mantle wedge sources. Plagioclase and garnet are preservers of Sr and HREE, respectively. Plagioclase is not stable, while garnet is a stable phase at higher grades of metamorphic facies. Rutile is a stable phase at higher metamorphic grades [20, 21]. High concentrations of Sr/Y, LREE/HREE, and LILE, and low concentrations of HFSE in adakites are attributed to the presence or absence of garnet, plagioclase, rutile, and amphibole in the subducted slab [1-9]. The positive correlation of Dy/Yb versus SiO₂ (Figure 9d) indicates the significant role of the garnet residual phase rather than the amphibole in the slab during the adakitic magma generation. The Ba/Th versus Nb/La diagram [61, 62] shows that most samples cluster around the lower pressure line (< 33 km) (Figure 9e). Low-pressure adakite generated by partial melting of the lower continental crust or differentiated from amphibole-dominated fractionation of calc-alkaline magma shows lower Ba/Th and $(\text{Sm}/\text{Yb})_{\text{SN}}$ compared the oceanic and orogenic adakites.

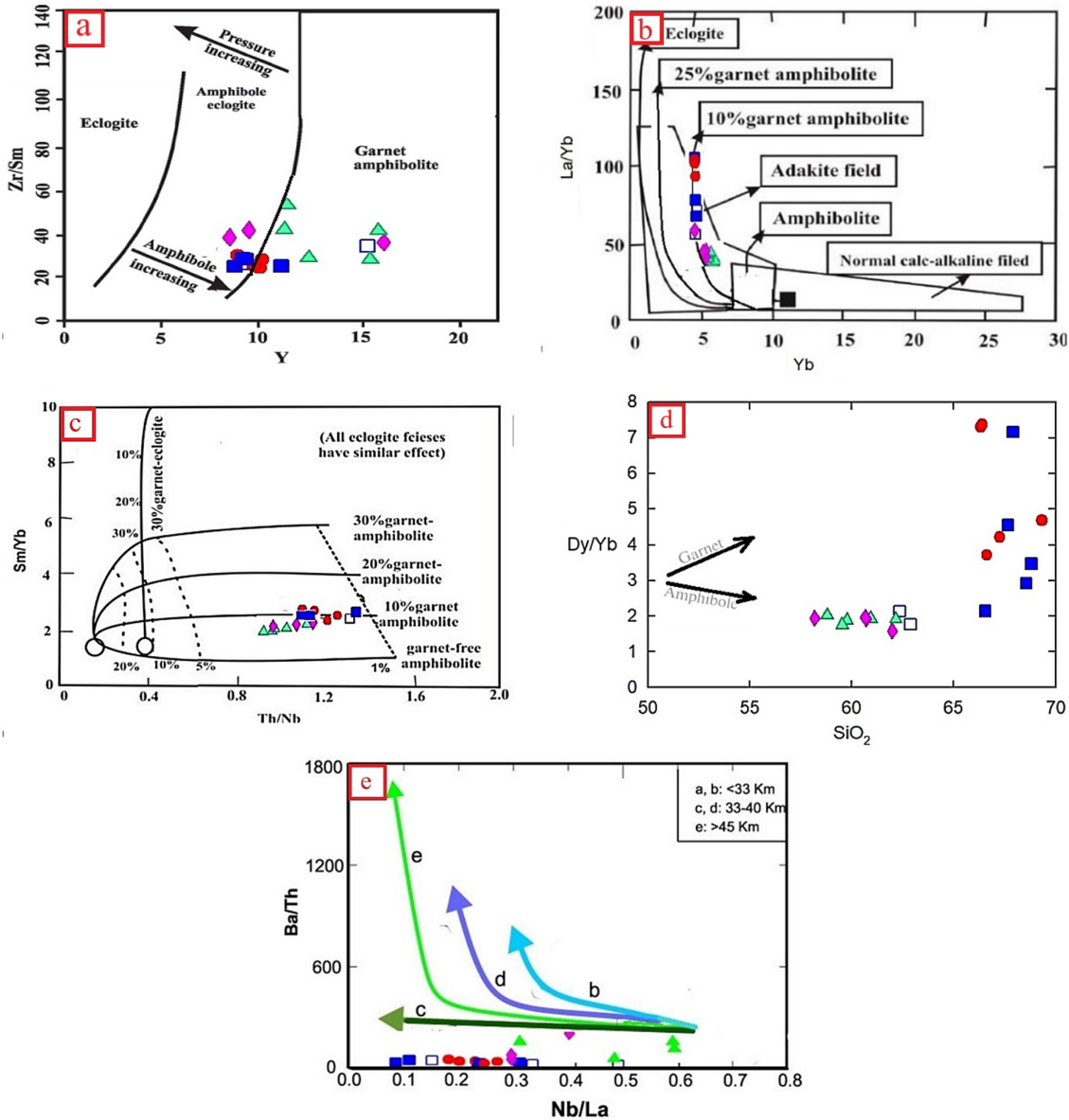


Figure 9. a) Diagram of Zr/Sm versus Y [63]; b) diagram of La/Yb versus Yb [45-52]; c) diagram of Sm/Yb versus Th/Nb [64]; d) bulk rock Dy/Yb versus SiO₂ (wt%) indicate residual garnet and amphibole during partial melting. The roughly flat pattern of samples indicates both garnet and amphibole as the residual minerals [65]; e) Ba/Th versus Nb/La diagram [61, 62].

The origin of adakitic magmas in the studied area was identified using the diagrams proposed in [65, 66]. These diagrams differentiate between adakites derived from the thickened crust, those resulting from the subduction of young and hot oceanic plates, and those originating from the metamorphic crust. As presented in Figure 10, the studied adakitic rocks fall within the melting range of subducted oceanic plates and the thickened lower crust. According to [67], partial melting of subducted sediments and oceanic plate-derived

liquids may induce metasomatism, and enrich the source area of subduction-related magmas. The melts from oceanic plate melting have high concentrations of U, Sr, Rb, Ba, and Pb, while partial melting of subducted sediments results in elevated concentrations of Th and LREEs. In normalized multivariate diagrams, these rocks exhibit significant LILE enrichment, and negative anomalies of Nb, Ti, and, to some extent, Ta. These results suggest that they were formed in a subduction-related tectonic environment.

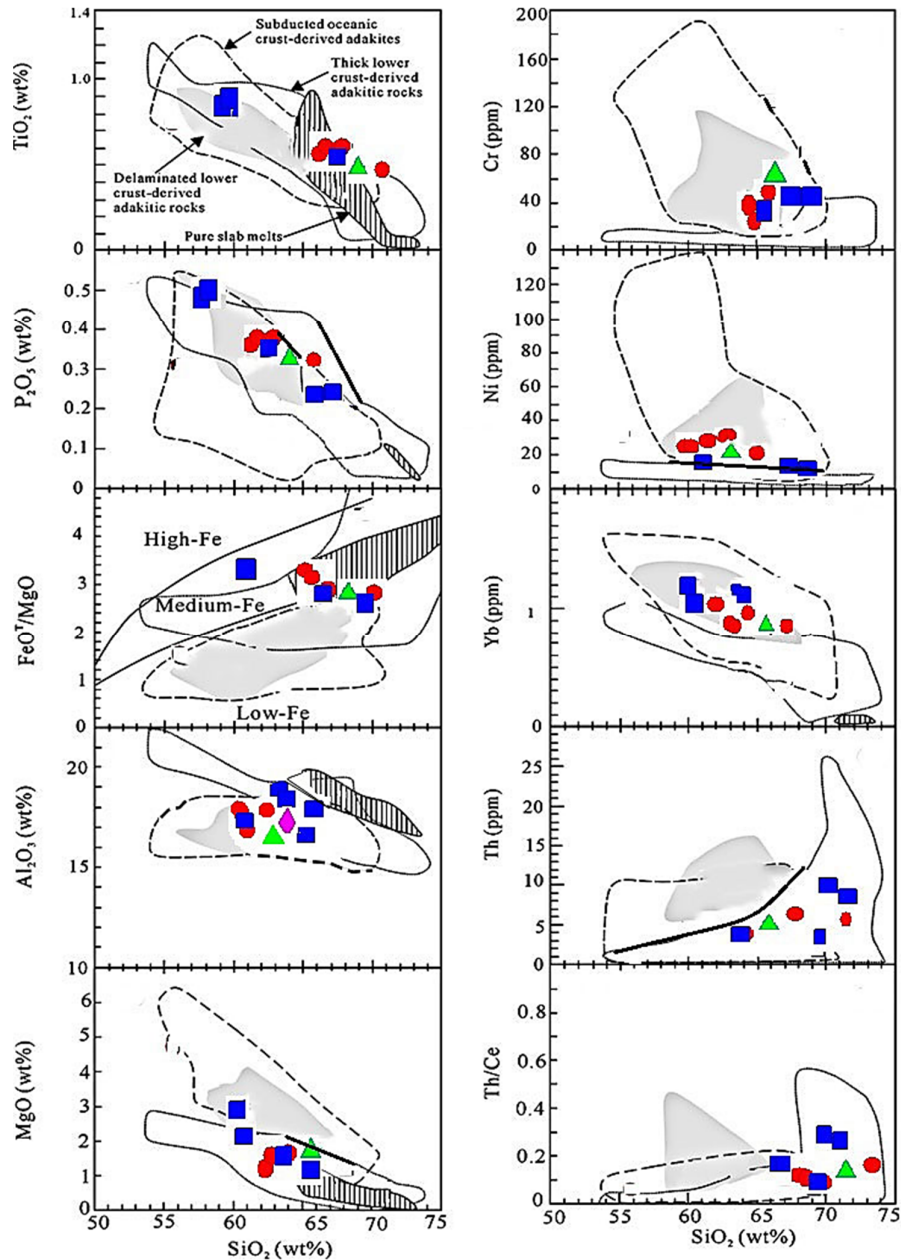


Figure 10. Diagrams illustrating the setting of the studied adakitic rocks, which are located within the melting range of subducted oceanic plates; the diagrams depict the field of adakitic rocks originating from the metamorphic lower crust (gray field), those originating from the subducted oceanic crust (dashed-line field), and those from the thickened lower crust (dotted-line field) and melt of the pure oceanic plate (shadow field) [68]; the diagram indicates the boundaries among igneous rocks with a low, intermediate, and high iron content [69].

Because of the high $D_{Zr, Nb}/D_{REE}$ in rutile [70, 71], Nb/La and Zr/Sm are expected to correlate if rutile is in control. Meanwhile, the presence of low Mg-amphibole (high D_{Nb}/D_{La} and low $D_{Zr, Nb}/D_{REE}$ [72] would cause these ratios to be inversely correlated. Melting of sources increases the Nb/Ta ratio in the generated melt compared with the amphibolite ones [72-74]. Also at the lower pressures of metamorphism, ilmenite controls the Nb-Ta content. However, rutile controls these

elements, and elevates the Nb/Ta ratio at higher pressures [74]. Superchondritic Nb/Ta values (> 20) in slab melt can be explained by residual rutile in the subducting plate without significant amounts of residual amphibole presence [72]. Figure 11 illustrates Nb/La and Nb/Ta versus Zr/Sm, highlighting the role of rutile, amphibole, or both as the residual phases on the HFSE control during slab melting. The roughly positive correlations of Nb/Ta versus Zr/Sm indicate that rutile was the

main factor of the fractionation of Nb from Ta (Figure 11a). The Nb/Ta ratio ranges from 5.31 to 16 (7.06, in average). There is a relationship between Nb/Ta and pressure. A research work has shown that the Shahneshin adakites are produced by partially melting subducted oceanic slabs at different depths (pressures) [75].

Adakites are remnant phases of garnet or amphibole at the site of their mafic genesis. There are three ways that adakitic magmas might originate in the subduction zones. These three formation processes are 1) partial melting of hot, young, subducted oceanic crust; 2) partial melting of thicker basaltic crust above the mantle wedge; and 3) partial melting of eroded continental crust

near the forearc of subduction [76]. Adakites associated with oceanic lithosphere subduction have a high magnesium number (#Mg), MgO, Cr, and Ni [77-79]. Investigating the geochemical characteristics of the studied adakites show that they originated from the melting of subducted oceanic plates.

Adakitic magmas have been reported in the adjacent areas of the studied region. These diagrams (Figure 11b) indicate that all the examined samples and samples from nearby regions are primarily the result of the partial melting of subducted oceanic plates in volcanic arcs.

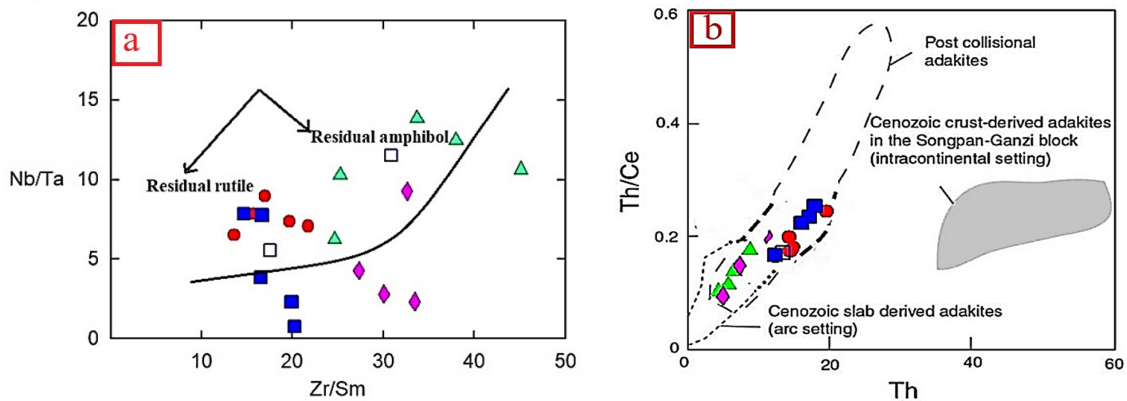


Figure 11. a) Nb/Ta versus Zr/Sm diagrams for the Shahneshin analytic samples; b) Th/Ce versus Th diagram; in these diagrams, the studied adakite samples are the product of subduction plate melting [80].

The Rb/Sr versus Sr/Y and Sr/Nb versus Gd/Yb diagrams were used to understand the role of sediments and fluids. The Rb/Sr versus Sr/Y diagram (Figure 12a) shows the effect of sediments on the subducting plate melt. In this respect, the studied samples are within the impact range of the subducting plate melt. Figure 12b presents the Sr/Nb versus Gd/Yb diagram, indicating the effect of the subducting plate fluids against the collapsible plate melts. As it can be seen, the studied samples are in the range of subducting plate melts. The orientation of the samples on these two diagrams suggests the dominant effect of subducting plate melt. The Rb concentration is usually affected by crustal components. In this regard, increasing the Rb/Sr ratio indicates the involvement of upper crustal and enriched mantle components [77-81]. The positive correlation between Sr/Nb and Gd/Yb indicates the components of the subducting plate at the origin. In the Rb/Y versus Nb/Y and Ba/Th versus Th discrimination plots, the adakite samples lie

between the slab-derived and melt-derived enrichment trends. Therefore, magmas might have originated from both the slab-derived fluids and melts (Figures 12C and 12D). The Sr/La ratio has been used to distinguish slab-derived adakites from those derived from the Lower Continental Crust (LCC), as altered oceanic crust (with MORB-type LREE depletion and Sr enrichment by seawater) has a much higher Sr/La ratio than the LCC [43]. Adakitic samples of the studied area have elevated Sr/La ratios (Figure 12a), suggesting a subducting oceanic slab-derived origin.

The results for the Sabalan indicate that the oceanic subduction-related adakitic magmas generally have higher contents of siderophile elements such as Ni = 1860 ppm, Co = 102 ppm, and Cr = 2520 ppm [83]. In the Al₂O₃-K₂O/Na₂O diagram, the adakites of the region have a high Al₂O₃ content and a low K₂O/Na₂O ratio, indicating the formation of these rocks from subduction-related crust [84] (Figures 13a and 13b).

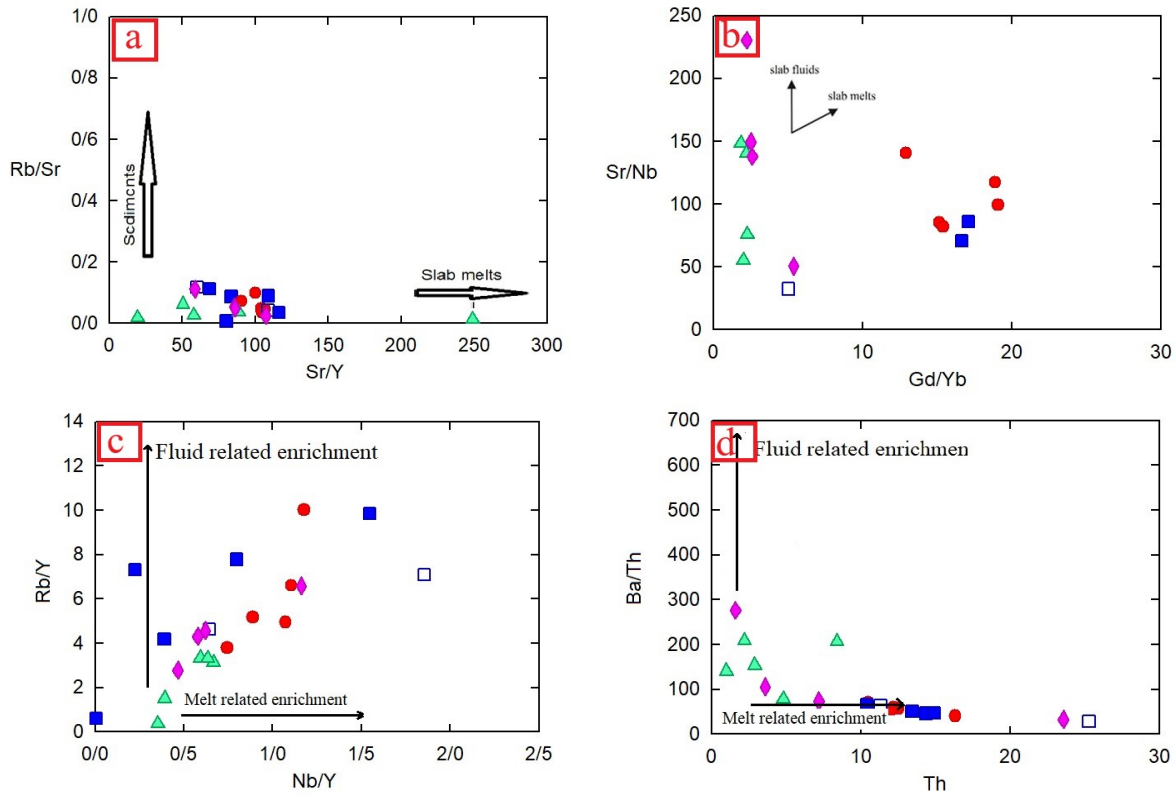


Figure 12. a) The Rb/Sr versus Sr/Y diagram [81]; b) the Sr/Nb versus Gd/Yb diagram [77]; c) and d) trace element plots for differentiating fluid-related versus melt-related enrichments [82].

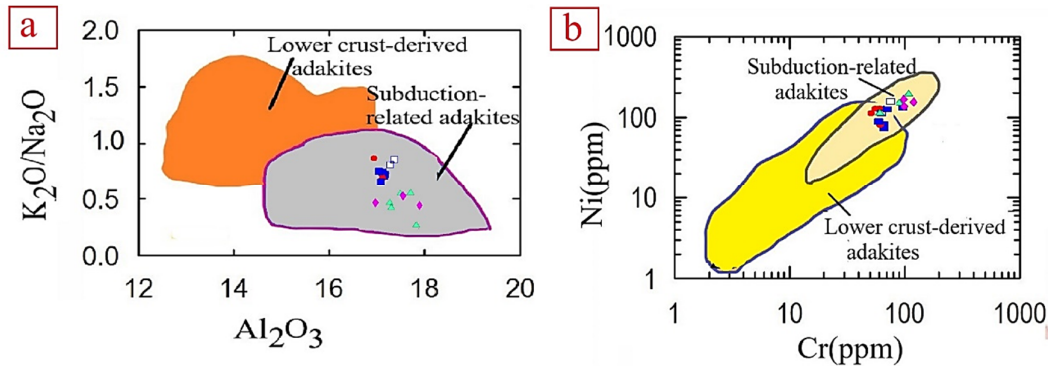


Figure 13. a) K_2O/Na_2O versus Al_2O_3 diagram [85] and b) Cr versus Ni diagram [86].

7. Nd-Sr Isotopes

Primary Sr and Ni isotopic ratios of the studied rock units are depicted in Table 4. As it can be seen, the amount of $\epsilon Nd(t)$ changes varies from +2.26 to +3.19, suggesting that the depleted mantle is the source of the melt [87]. The adakitic rocks of the studied area, which also show relatively high ϵNd values, overlap with the rocks of other Late Miocene-Quaternary impact volcanoes in northwest Iran, east Türkiye, and the Little Caucasus show. Adakite rocks that have strongly negative Nd isotopic compositions are derived from the ancient mafic lower crust (e.g. $\epsilon Nd(t) \sim -$

5 to -10) [88, 89]. In contrast, adakitic rocks with positive Sr-Nd isotopic compositions are often derived from the young basaltic crust (e.g. $\epsilon Nd(t) = +1$ to +6) [90, 91]. The adakitic rocks in the studied area display moderately positive $\epsilon Nd(t)$ values (+2.26 to +3.19), and young TDM (Nd) (395-465 Ma). The Sr isotopic studies [92] indicate that the composition changes of the $^{87}Sr/^{86}Sr$ isotope ratio of the volcanic rocks of the studied area are between 0.7035 and 0.7060. These values are attributed to the heterogeneity of the mantle and different degrees of crystallization, which play a major role in the formation of calc-alkaline

magmas. The parent magmas (calc-alkaline) of these rocks result from dehydration of the oceanic crust at a high water vapor pressure and a high oxygen pressure [93]. In this process, by melting, the mantle wedge is above the subduction zone and without the participation of the sialic continental crust [92].

According to the isotopic ratios and Figures 15 and 14, the adakites of the studied area are obtained from the melting of subducted oceanic crust in a tensile environment. In this context, the Sr isotopic

studies [92] indicate that the composition changes of the $^{87}\text{Sr}/^{86}\text{Sr}$ isotope ratio of the volcanic rocks of the studied area are between 0.7035 and 0.7060. These values are explained by the heterogeneity of the mantle and different degrees of crystallization, which play a major role in the formation of calc-alkaline magmas. Adakites in the studied area are not directly derived from the partial melting of the underlying mafic crust because they contain relatively low amounts of MgO, Cr, and Ni [94, 95].

Table 4. Whole rock Sr-Nd analysis for the Shahneshin adakitic rocks.

Rock type	Dacite	Rhyodacite	Dacite	Rhyodacite	Rhyodacite
Samples	20t	S27T	S6-A	S29T	S40T
$^{87}\text{Sr}/^{86}\text{Sr}$	0.7041	0.7043	0.7042	0.7044	0.7048
$^{143}\text{Nd}/^{144}\text{Nd}$	0.5128	0.5127	0.5129	0.5129	0.5127
ϵNd	2.81	2.26	2.98	2.71	3.19
TDM	395	465	425	470	461

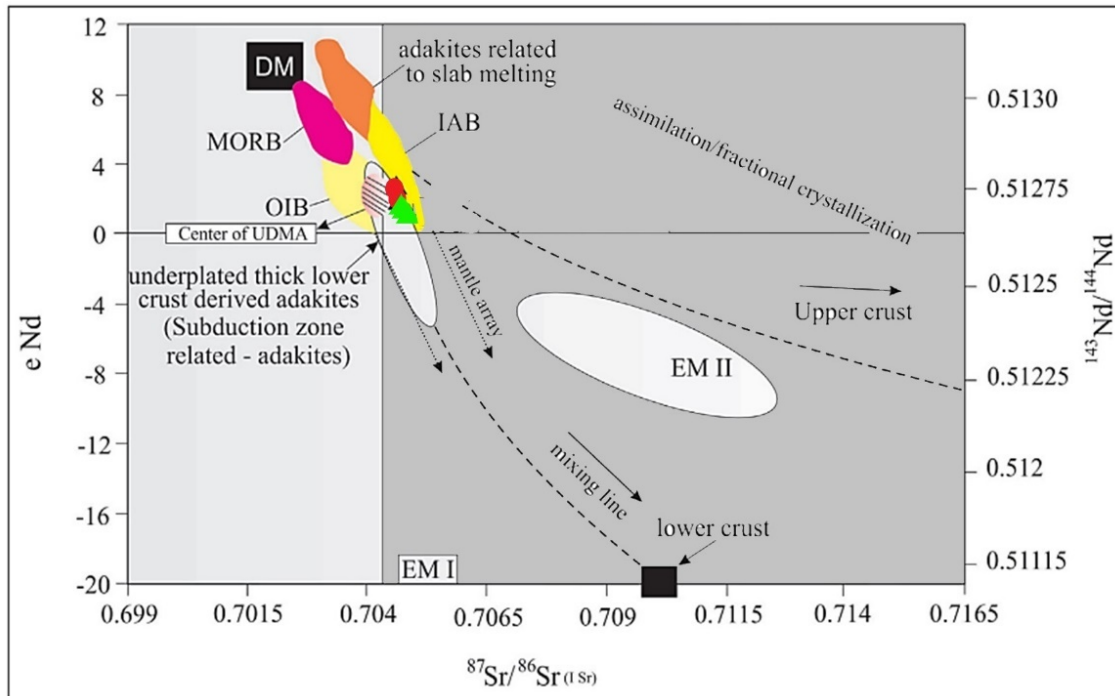


Figure 14. The diagram of ϵNd versus $^{86}\text{Sr}/^{87}\text{Sr}$ [86] illustrates the dependence of the studied samples on the subduction zone and the tendency for staining of skins and meats (classifications of IAB, DM, MORB, and EM from [96]). The distribution of adakites related to the oceanic sheet is from [97], while the distribution of adakites is related to the thick lower crust is from [98, 99], respectively, for the southern and central UDMA [100].

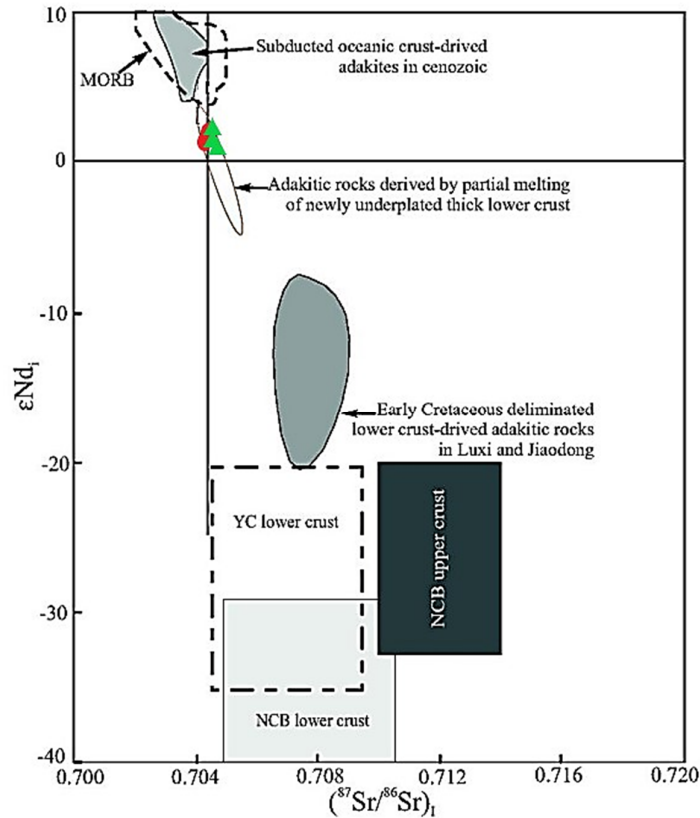


Figure 15. The diagram of ϵNd_i versus $^{86}Sr/^{87}Sr$ is a combination of the diagram proposed by [43-101].

8. Geodynamic Setting

In the recent years, several studies have introduced adakite melts, and explained their genesis in the Azarbaijan zone [85-102]. Below are some perspectives on the formation of adakites:

1. Melting of the subducting oceanic crust [45-52-103, 104]: partial melting of the subducted oceanic crust typically generates adakitic magma with a high Si, Al, and Sr (> 400 ppm), a high Sr/Y ratio (> 20), and a low Y (20), along with a depleted Sr-Nd isotopic composition ($^{87}Sr/^{86}Sr < 0.705$, $\epsilon Nd > 4$) [105, 106-45].
2. Melting of the continental crust base [107-112]
3. Fractional crystallization of arc parent magma [49, 113-116]
4. Transpressional differentiation from the water-bearing mantle melt [117-120]
5. Mixing of evolved magmas with primary mantle magmas in shallow magmatic chambers [49]

In general, two sources have been suggested for adakitic melts in the Azarbaijan region:

- 1) Melting of the subducted oceanic plate under the conditions of amphibolite-eclogite facies. For example, Neogene adakitic magmatism was

introduced in different regions of Azerbaijan with amphibole-eclogite to the garnet-eclogite origin of the subducted oceanic lithosphere of Neo-Tethys, and in a post-collision position [121]. Furthermore, Pelio-quaternary dacitic volcanic rocks in the north of Sahand volcano were considered adakitic magmatism associated with melting the ruptured oceanic plate of Neo-Tethys [122].

- 2) Melting of the lower continental crust; for instance, regarding the chemical and isotopic properties, the origin and location of the adakitic rocks in the southeast of Julfa are attributed to the melting of the lower part of the thickened continental crust [123].

Since the adakites or adakitic melts are not provided by simply melting the subducted plate, other processes are required for their formation. Adakites produced by the subduction of oceanic crust vary from those produced by lower crustal melting and delamination. Compared with the other two categories, adakitic rocks from lower crust melting have a larger FeOt/MgO ratio, Al_2O_3 , and a Th/Ce ratio, and a lower concentration of compatible elements like Cr, Ni, and MgO. Another noteworthy point is that the lower crustal adakitic melt discharged into the mantle has more

compatible elements like Cr, Ni, and MgO than the upper crustal adakitic melt. This difference leads to the interaction of the melt with the mantle, and enhances the concentration of its compatible elements [1-58]. The adakitic melts from the lower crust left in the mantle do not have a strong geochemical affinity with the samples in the research work region. Besides, although suitable elements like Ni are more abundant in the examined samples than in the adakitic melts coming from the lower crust, the MgO and Cr concentrations are not proportionate to those of the adakitic melts originating from the subducting oceanic crust. These elements outperform the adakites produced by melting the lower crust and the Th/Ce ratio in the area samples. Similarly, lower crust-derived adakites have greater Rb and K_2O/Na_2O ratios than adakites from subducted plates [124]. Th, Rb, and K_2O/Na_2O in the subducted plate adakites are 4.5 ppm, 41 ppm, and 0.35, respectively, while they are 13.48 ppm, 61.71 ppm, and 0.70 for the adakite originating from melting the lower crust in the studied area [51]. Assuming the lower crust origin for adakites' genesis, some researchers have considered the existence of a large crust (thicker than 50 km) as a necessary precondition [66-68, 81-125]. However, experimental studies have shown that partial melting of the lower mafic crust at a depth of 30 to 40 km and a temperature of 800 to 900 °C can produce Adakit melts, and the lower crust does not need to undergo the conditions of the eclogite facies [126]. Geophysical studies in northwestern Iran indicate that the crust of this area is more than 40 km thick [127]. The thickness of the crust is unlikely to be an obstacle to producing adakitic melt in the Azerbaijan region. Considering the high depletion of HREEs (e.g. Yb) in the adakitic melt of the region, the considerable thickness of the crust probably stabilizes garnet (eclogite facies) at the base of the crust. Geophysical studies reveal lithosphere thinning (between 100 and 85 km) in northwest Iran [23, 128, 129]. The whole thickness of the lithosphere is less than the considerable crust thickness in Azerbaijan (more than 40 km). Previous studies have noted and debated a thin lithosphere for this area, but general geophysical research work in Azerbaijan, and the Iranian-Turkish plateau provides evidence of a thick lithosphere [27]. One of the anticipated tectonic impacts of the plates' post-collision is the thickening of the lithosphere. Hence, according to the discussions about the collision of the Arabian-Eurasian plates in the late Eocene-Oligocene [130-132], the thickening of the lithosphere, and the

subducted slab break-off are expected after this time. In general, the process of tectonic evolution continues after the lithosphere thickening, the lithosphere base break-off, and its re-thinning. As a result, these factors lead to asthenospheric ascension, and increased heat flow. In the northwestern region of the Iran-Caucasus-Turkey plate, the lithosphere base has been broken off, and the asthenosphere has risen in the Neogene [27-133]. Consequently, the lithosphere has melted [134], leading to a widespread magmatism.

Notably, other tectonic occurrences such as the break-off of a subducted slab may also lead to the emergence of a new phase of magmatism. The Neogene-Quaternary magmatism's spatial and temporal irregularity in Azerbaijan is among the contradictory aspects related to the melting of the subducted plate. Since no specific spatial pattern is observed regarding the age and chemical composition of magmatism in Azerbaijan, the partial melting of the underplate is a more logical process for generating adakitic melts in the region [133]. Overall, various processes related to Neogene magmatism in Azerbaijan can be summarized as follows:

1. Processes associated with the active subduction zone (post-collision) cause mantle wedge metasomatism in terms of the subducted plate materials. Some of the melt produced at this stage may have accumulated at the base of the continental crust, and mafic rocks have formed the mafic underplates.

2. In the post-collision (Neogene) phase, which may have been accompanied by subduction oceanic lithosphere break-off [27], break-off, or melting of the continental asthenospheric underplate, and its thinning have occurred with lateral flows and asthenospheric mantle uprising. At this stage, the high heat flow of the mantle occurred concerning the asthenospheric mantle ascension and the lithospheric thinning. This flow has led to the melting of the lithosphere and the underplate mafic rocks (i.e. the source of adakitic magmatism). Alkaline melts in Azerbaijan may be caused by asthenospheric mantle melts or by partially melting the lithospheric mantle [135]. After adakites, alkaline melts with shoshonitic, lamprophyritic, and alkaline ultrasonic potash as part of their makeup erupt [3]. The Miocene Saray and Sahand alkaline eruptions are among the notable instances of this event [136, 135]. Besides, several cases of Neogene (Pliocene-Quaternary) alkaline magmatism were reported in different parts of northwestern Iran [133-137]. In northeastern Türkiye (Eastern Pontid), it is

believed that Pliocene alkaline magmatism has followed the Miocene Adakitic magmatism. The origin of alkaline magmatism was linked with the asthenospheric uplift and melting of the metasomatized mantle [138]. The produced adakitic melt may have contaminated the mantle melt, thereby increasing the concentration of some compatible elements (e.g. Ni) in the adakitic melt. One of the characteristics of magmatism at this stage is the chemical diversity of the melt due to different mantle origins, crustal contamination, and fractional crystallization processes. Besides, the lithospheric underplate break-off agrees with the geophysical studies and the spatial distribution of eruptions in a wide area (northwestern Plateau of Iran-Turkey) [27].

Some researchers proposed that the Neo-Tethyan oceanic crust rolled back after the subduction, and finally, separated in the Upper Miocene or the middle to late Eocene [11, 139-142].

In [143-145], the northwest geothermal area of Sabalan was investigated using the data and results from the surface and sub-surface investigations including geology, geophysics, hydrogeochemistry, and hydrology. The findings revealed the presence of geothermal energy in the northwest of Sabalan. Various models were examined, and ultimately, the best model of the natural state demonstrated a high flow of fluid with high temperatures in the southern part of the region, with a change rate of 108 kg/s. Numerical and thermodynamic modeling to estimate the production capacity of the northwestern Sabalan geothermal field in Iran showed that the main factors controlling this capacity were the expected pressure drop and the enthalpy of the production fluid. This field can provide sufficiently a high-enthalpy fluid for a maximum capacity of 114 MW for 70 years [143-145].

In the area of Azarbaijan, remnants of subducted oceanic crust are trapped in the Eurasian underplate. The basaltic rocks of the Neo-Tethys oceanic crust have changed into amphibolite, and, finally, eclogite due to subduction and related metamorphism. This mechanism metasomatized the lithosphere mantle, and produced fluids or partial melts rich in LILE and LREE. The parent magma of the Shahneshin volcano was generated by intense partial melting of the metasomatized mantle, which took on the traits of a subducted oceanic crust. This concept is consistent with the hypotheses that have been put up in the past regarding post-collision calc-alkaline magmatism in Iran. In this regard, lower crustal stratification

[131, 134, 144] has been proposed for Upper Cenozoic magmatism in eastern Turkey and northeastern Iran in the research work of young volcanoes in southern Turkey. In addition, the researchers [145] claim that the oceanic crust of Neo-Tethys below the Eurasian plate has triggered the Quaternary magmatism in this region. In [134], the delamination process for eastern Anatolia and northwestern Iran was proposed. According to studies, the upper mantle temperature in parts of Iran is higher than that of its solidus temperature. Thus it is characterized by a decrease in shear wave velocity, a decrease in density, and the occurrence of volcanism (in the Quaternary). Accordingly, it is believed that the delamination process has reduced the cold materials and replaced them with hot mantle materials. At this time, the activity of some strike-slip faults has caused tensile basins, and transported depleted asthenospheric material to higher levels. New studies show that tensile spaces are still expanding along some of the strike-slip faults of the area (e.g. the north Tabriz fault) [146], and generated enriched products. In some cases, the cold lithosphere has reached its melting point in terms of pressure reduction and proximity to the hot mantle, producing richer products. Meanwhile, the metasomatism process (i.e. fluids generated due to the oceanic lithosphere subduction) has declined the melting point of the lithosphere and the upper mantle.

Shahneshin volcano is located in a compressive tectonic setting. The current deformation pattern of Shahneshin shows that the tectonic stress regime has experienced different magmatic tectonics. The predominant direction of the lines in Shahneshin is N-S and NW-SE. These lines are arranged radially in the new Shahneshin sediments with a dominant N-S direction. In the area of the Shahneshin volcano, the density of volcanic domes around the Kasra peak is higher (Figure 16). Considering their young age, it seems that a pull-apart basin between the right-slip faults of Alvarez and Khiavachai-Moeel bedrock was effective in their eruption. Hence, according to the recent structural studies of fractures and fault trends in Shahneshin Mountain, it is concluded that the performance of strike-slip faults has created tensile spaces and pull-apart basins in the region (Figure 16). During the Quaternary, the region-playing magmas reached the Earth's surface along with these tensile spaces.

These magmas were slightly contaminated with the lithospheric crust, and have largely retained their asthenospheric characteristics. In general, these magmas are alkaline, and depleted REEs. In the next stage, the lithospheric crust underwent a

delamination process, and a part of it was separated from the crust and immersed in the asthenosphere. Meanwhile, partial melting of this crust has caused the formation of adakites in Shahneshtin.

In [19], a model was proposed for the 3 volcanoes, Sabalan, Sahand, and Saray. This model shows that the parental magma from a mantle source originated from metasomatic agents related to enriched subduction. In line with their extreme enrichment in incompatible elements and their marked Sr- and Pb-radiogenic, and Nd-unradiogenic composition, the thickness of the mantle wedge is expected to increase from southwest to northeast. Thus the relative volume of metasomes decreases in the same direction from Saray to Sabalan (Figure 14).

In studying the Sahand volcano [147], two types of magma were identified from the Miocene-Quaternary period: "normal" calc-alkaline, mantle-derived melts, and "adakitic" lower-crustal derived melts. This model is also applicable to the Sabalan volcano. In this model, the magma originates from the mantle due to the breaking of the subducted slab or due to the opening of the slab tear. The subsequent gradual onset of magmatism at increasing distances from the suture zone is

attributed to the propagating thermal pulse. In the studied area, a highly variable magmatism is observed. This magma ranges from high-K near-primitive melt (at Saray) to the magmatic activity of non-adakitic paired adakites (Sahand) and adakitic magmatism (Sabalan). Here, the crustal thickness increases progressively [147]. Adakites have also been reported in eastern and central Iran. The Lakhshak plutonic complex (Adakite) in east Iran is consistent with an origin from oceanic slab melts variously mixed with melts from flysch sediments [151].

The source for the adakitic rocks of the Torud-Ahmadabad magmatic belt is a subducted Neo-Tethys oceanic slab and mantle metasomatism in the SSZ. The late Eocene voluminous magmatism appears to be associated with local extension (transpression) in the continentally situated arc setting evolving into rifting in the Neogene. This setting may be caused by slab rollback or breakoff coincident with upwelling asthenospheric mantle throughout this period. The adakitic magma in the Sabzevar ophiolitic zone was obtained from partial wet melting of the garnet amphibolite source from the subducted oceanic shale of Sabzevar.

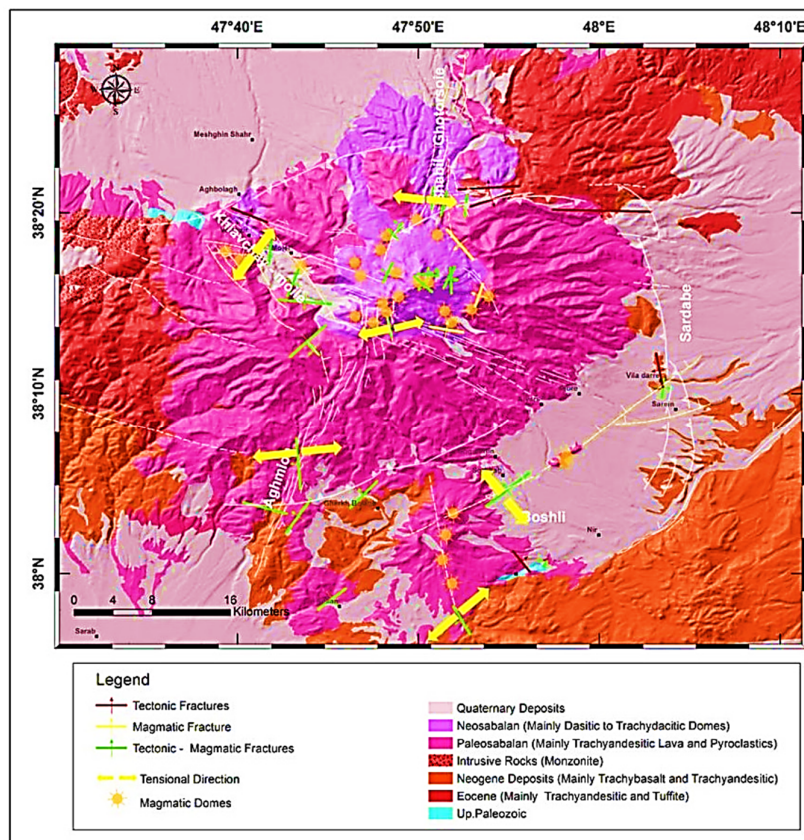


Figure 16. A simplified geological map along with the direction of the fractures (thick yellow arrows for tension direction and arrows along the fracture for the fracture slope) overlays on the SRTM images [151].

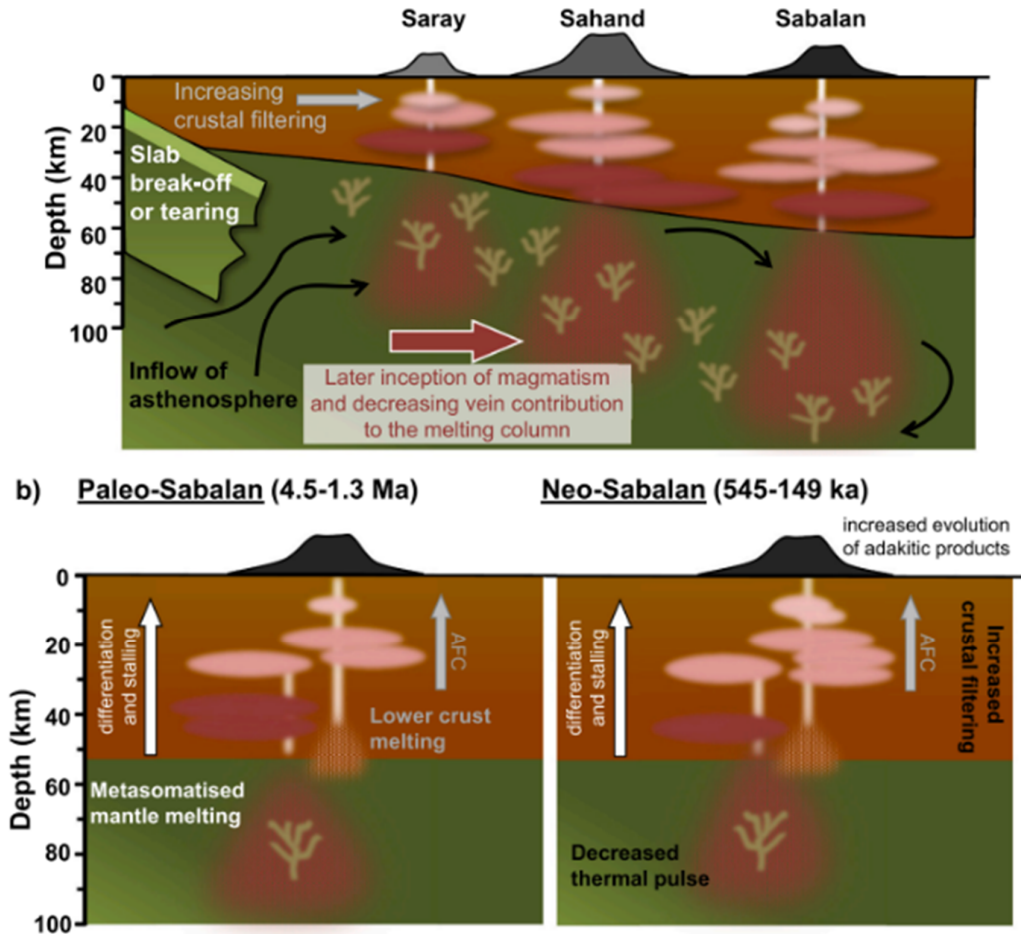


Figure 17. a) Post-collisional stages along the Saray-Sahand-Sabalan array (not to scale) and b) the schematic representation of the proposed conceptual model for the evolution of magmatism at Sabalan volcanoes (not to scale) [149].

9. Conclusions

The three stratovolcanoes Saray, Sahand, and Sabalan (Shahneshin) in northwestern Iran are located at increasing distances of approximately ~140 km and ~300 km from the Neo-Tethyan suture zone. The Shahneshin volcanic complex feature rocks of basaltic andesite, andesite, trachyandesite, and dacite compositions. All Shahneshin adakitic samples exhibit characteristics typical of adakites including a high Sr/Y ratio, elevated LREE/HREE, depleted HFSE (Ta, Nb, and Ti), and enrichment of LILE. Nb/Ta variations in the Shahneshin adakitic rocks indicate slab melting at different depths. The Dy/Yb ratio indicates the role of both garnet, and amphibole in adakitic magma generation. The high Dy/Yb ratio shows a positive correlation with SiO₂, suggesting the presence of garnet as a refractory phase during slab melting.

Conversely, a negative correlation of Dy/Yb with SiO₂ content indicates that amphibole (unlike

garnet) serves as a refractory phase during slab melting. Considering the collision of the Arabian-Eurasian continental plates and the closure of the Neo-Tethys in pre-Miocene times, along with current geophysical evidence, several events (e.g. the subducted slab break-off, asthenospheric uplift, and the break-off of thickened underplate lithosphere) have occurred during the post-collision period. These processes can lead to the melting of the metamorphic crust and mantle, resulting in various magmatic activities with a relatively wide spatial distribution, extending from the northwestern part of Iran to eastern Turkey during the Neogene period.

References

- [1]. Martin, H., Smithies, R., Rapp, R., Moyen, J. F., & Champion, D. (2005). An overview of adakite, tonalite-trondhjemite-granodiorite (TTG), and sanukitoid relationships and some implications for crustal evolution. *Lithos*, 79(1-2), 1-24.

- [2]. Zhang, P. Z., Wen, X. Z., Shen, Z. K., & Chen, J. h. (2010). Oblique, high-angle, listric-reverse faulting and associated development of strain: The Wenchuan earthquake of May 12, 2008, Sichuan, China. *Annual review of earth and planetary sciences*, 38, 353-382.
- [3]. Jahangiri, A. (2007). Post-collisional Miocene adakitic volcanism in NW Iran: geochemical and geodynamic implications. *Journal of Asian Earth Sciences*, 30(3-4), 433-447.
- [4]. Ghorbani, M. R., & Bezenjani, R. N. (2011). Slab partial melts from the metasomatizing agent to adakite, Tafresh Eocene volcanic rocks, Iran. *Island Arc*, 20, 188-202
- [5]. Azizi, H., Asahara, Y., Tsuboi, M., Takemura, K., & Razyani, S. (2014). The role of heterogenetic mantle in the genesis of adakites northeast of Sanandaj, northwestern Iran. *Chemie der Erde-Geochemistry*, 74, 87-97.
- [6]. Delavari, M., Amini, S., Schmitt, A. K., McKeegan, K. D., & Harrison T. M. (2014). U-Pb geochronology and geochemistry of Bibi-Maryam pluton, eastern Iran: Implication for the late stage of the tectonic evolution of the Sistan Ocean. *Lithos*, 200, 197-211.
- [7]. Rossetti, F., Nasrabad, M., Theye, T., Gerdes, A., Monié, P., Lucci, F., & Vignaroli, G. (2014). Adakite differentiation and emplacement in a subduction channel: The late Paleocene Sabzevar magmatism (NE Iran). *GSA Bulletin*, 126, 317-343.
- [8]. Omrani, H. (2018). Island-arc and active continental margin adakites from the Sabzevar zone, Iran. *Petrology*, 26, 96-113.
- [9]. Castillo, P. R. (2006). An overview of adakite petrogenesis. *Chinese Science Bulletin*, 51, 257-268.
- [10]. Şengör, A. M. C., & Kidd, W. S. F. (1979). Post-collision tectonics of the Turkish and Iranian plateau and companions with Tibet. *Tectonophysics*, 55, 361-376.
- [11]. Dewey, J. F., Hempton, M. R., Kidd, W. S. F., Şaroğlu, F., & Şengör, A. M. C. (1986). Shortening of continental lithosphere: The neotectonics of Eastern Anatolia a young collision zone. Coward, M., Ries, A.(Ed.). *Collision Tectonics. Special Publication of the Geological Society. London*, 19, 3-36.
- [12]. Dilek, Y., & Altunkaynak, Ş. (2009). Geochemical and temporal evolution of Cenozoic magmatism in Western Turkey: mantle response to collision, slab break-off, and lithospheric tearing in an orogenic belt. *Geological Society of London Special Publication*, 311, 213-233.
- [13]. Kheirkhah, M., Allen, M. B. & Emami, M. (2009). Quaternary syn-collision magmatism from the Iran/Turkey borderlands, *Journal of Volcanology and Geothermal Research*, 182(1-2), 1-12.
- [14]. Azizi, H., & Tsubo, M. (2021). The Van Microplate: A New Microcontinent at the Junction of Iran, Turkey, and Armenia. *Frontiers in Earth Science*, 8.
- [15]. Allen, M. B., Kheirkhah, M., Neill, I., Emami, M. H., & McLeod, C. L. (2013). Generation of arc and within-plate chemical signatures in collision zone magmatism: quaternary lavas from Kurdistan province, Iran. *Journal of Petrology*, 54(5), 887-911.
- [16]. Chiu, H.Y., Chung, S.L., Zarrinkoub, M.H., Mohammadi, S.S, Khatib, M.M., & Iizuka, Y. (2013). Zircon U-Pb age constraints from Iran on the magmatic evolution related to Neotethyan subduction and Zagros orogeny. *Lithos*, 162(24), 70-87.
- [17]. Ghalamghash, J., Schmitt, A.K., & Chaharlang, R. (2019). Age and compositional evolution of Sahand volcano in the context of postcollisional magmatism in northwestern Iran: evidence for time transgressive magmatism away from the collisional suture. *Lithos*, 344-345, 265-279.
- [18]. Lustrino, M., Salari, G., Rahimzadeh, B., Fedele, L., Masoudi, F., & Agostini, S. (2021). Quaternary melanephelinites and melilitites from Nowbaran (NW Urumieh-Dokhtar Magmatic Arc, Iran): origin of ultrabasic-ultracalcic melts in a post-collisional setting. *Journal of Petrology*, 62, 1-31.
- [19]. Fedele, L., Mehdipour Ghazi, J., Agostini, S., Ronca, S., Innocenzi, F., & Lustrino, M. (2023). Concurrent adakitic and non-adakitic Late Miocene-Quaternary magmatism at the Sahand volcano, Urumieh-Dokhtar Magmatic Arc (NW Iran). *Lithos*, 458-459, 107344.
- [20]. Omrani, H., Michaeli, R. & Moazzen, M. (2013). Geochemistry and petrogenesis of the Gasht peraluminous granite, western Alborz Mountains, Iran. *Neues Jahrbuch für Geologie und Paläontologie - Abhandlungen*, 268/2, 175-189.
- [21]. Omrani, H., Moazzen, M., Oberhänsli, R., Tsujimori, T., Bousquet, R. & Moayyed, M. (2013). Metamorphic history of glaucophane-paragonite-zoisite eclogites from the Shanderman area, northern Iran. *Journal of Metamorphic Geology*, 31, 791-812.
- [22]. Omrani, H., Moazzen, M., Oberhänsli, R., & Moslempour, M. E. (2017). Iranshahr blueschist: subduction of the inner Makran oceanic crust. *Journal of Metamorphic Geology*, 35(4).
- [23]. Bavali, K., Motaghi, K., Sobouti, F., Ghods, A., Abbasi, M., Priestley, K., & Rezaei, M. (2016). Lithospheric structure beneath NW Iran using regional and teleseismic travel-time tomography. *Physics of the Earth and Planetary Interiors*, 253, 97-107.
- [24]. Faridi, M., Nazari, H., Burg, J. P., Haghipour, N., Talebian, M., Ghorashi, M., & Sahebari, S. S. (2019). Structural Characteristics, Paleoseismology and Slip Rate of the Qoshadagh Fault, Northwest of Iran. *Geotectonics*, 53(2), 280-297.

- [25]. Moradi, A. S., Hatzfeld, D., & Tatar, M. (2011). Microseismicity and seismotectonics of the North Tabriz fault (Iran). *Tectonophysics*, 506(1-4), 22-30.
- [26]. Azad, S. S., Philip, H., Dominguez, S., Hessami, K., Shahpasandzadeh, M., Foroutan, M., & Lamothe, M. (2015). Paleoseismological and morphological evidence of slip rate variations along the North Tabriz fault (NW Iran). *Tectonophysics*, 640, 20-38.
- [27]. Dilek, Y., Imamverdiyev, N., & Altunkaynak, Ş. (2010). Geochemistry and tectonics of Cenozoic volcanism in the Lesser Caucasus (Azerbaijan) and the peri-Arabian region: collision-induced mantle dynamics and its magmatic fingerprint. *International Geology Review*, 52(4-6), 536-578.
- [28]. Ghalamghash, J., Mousavi, Z., Hassanzadeh, J., & Schmitt, A. K. (2016). Geology, Zircon geochronology and petrogenesis of Sabalan Volcano: northwest Iran. *Journal of Volcanology and Geothermal Research*, 327, 192–207.
- [29]. Ghalamghash, J., Mousavi, S.Z., & Khalatbari Jafari, M. (2022). Thermobarometry and petrogenesis of Sabalan volcanic rocks: based on mineral chemistry. In Persian. *Researches in Earth Sciences*, 13, 26–43.
- [30]. Verdel, C., Wernicke, B.P., Hassanzadeh, J., & Guest, B. (2011). A Paleogene extensional arc flare-up in Iran. *Tectonics*, 30(3).
- [31]. Mason, J. A., Jacobs, P. M., Hanson, P. R., Miao, X., & Goble, R. J. (2003). Sources and paleoclimatic significance of Holocene Bignell loess, central Great Plains, USA. *Quaternary Research*, 60(3), 330-339.
- [32]. Didon, J., & Gemain, Y. M. (1976). Le Sabalan, volcan plio-quaternaire de l'Azerbaïdjan oriental (Iran): étude géologique et pétrographique de l'édifice et de son environnement régional. Université Scientifique et Médicale de Grenobl.
- [33]. Shahbazi Shiran, H. (2013). Petrogenesis of Quaternary Shoshonitic Volcanism in NE Iran (Ardabil): Implication for Postcollisional Magmatism. *Journal of Geological Research*, 1-12.
- [34]. Le Bas, M. J., Le Maitre, R. W., Streckeisen, A. & Zanettin, B. (1986). A chemical classification of volcanic rocks based on the total alkali-silica diagram. *Journal of Petrology* 27(3), 745-750.
- [35]. Hastie, A. R., Kerr, A. C., Pearce, J. A., & Mitchell, S. (2007). Classification of altered volcanic island arc rocks using immobile trace elements: development of the Th–Co discrimination diagram. *Journal of petrology*, 48(12), 2341-2357.
- [36]. Irvine, T. N., & Baragar, W. (1971). A guide to the chemical classification of the common volcanic rocks. *Canadian journal of earth sciences*, 8(5): 523-548.
- [37]. Peccerillo, A., & Taylor, S. R. (1976). Geochemistry of Eocene Calc-alkaline volcanic rocks from the Kastamonu area. Northern Turkey Contrib, *Mineral Petrology*, 58(1), 63–8.
- [38]. Sun, S. S. & McDonough, W. S. (1989). Chemical and isotopic systematics of oceanic basalts: implications for mantle composition and processes. *Geological Society*, 42(1), 313-345.
- [39]. Drake, M. J., & Weill, D. F. (1975). Partition of Sr, Ba, Ca, Y, Eu²⁺, Eu³⁺, and other REE between plagioclase feldspar and magmatic liquid: an experimental study. *Geochimica et Cosmochimica Acta*, 39(5), 689-712.
- [40]. Weill, D. F., & Drake, M. J. (1973). Europium anomaly in plagioclase feldspar: experimental results and semiquantitative model. *Science*, 180(4090), 1059-1060.
- [41]. Lai, S., Qin, J., Li, Y., Li, S., & Santosh, M. (2012). Permian high Ti/Y basalts from the eastern part of the Emeishan Large Igneous Province, southwestern China: Petrogenesis and tectonic implications. *Journal of Asian Earth Sciences*, 47, 216-230.
- [42]. Irving, A. J., & Frey, F. A. (1978). Distribution of trace elements between garnet megacrysts and host volcanic liquids of kimberlitic to rhyolitic composition. *Geochimica et Cosmochimica Acta*, 42(6), 771-787.
- [43]. Liu, S., Hu, R. Z., Gao, S., Feng, C. X., Yu, B. B., Qi, Q., Wang, T., Feng, G. Y., & Coulson, I. M. (2009). Zircon U-Pb age, geochemistry and Sr-Nd-Pb isotopic compositions of adakitic volcanic rocks from Jiaodong, Shandong province, eastern China: constraints on petrogenesis and implications. *Journal of Asian Earth Sciences*, 35(5), 445-458.
- [44]. Kepezhinskas, P. K., Defant, M. J., & Drummond, M. (1995). Na metasomatism in the island-arc mantle by slab melt–peridotite interaction: evidence from mantle interaction-evidence from mantle xenoliths in the north Kamchatka arc. *Journal of Petrology*, 36, 1505–1527.
- [45]. Defant, M.J., Drummond, M.S. (1990). Derivation of some modern arc magmas by melting of young subducted lithosphere. *nature*, 347(6294), 662-665.
- [46]. Fraser, G., Ellis, D., & Eggins, S. (1997). Zirconium abundance in granulite-facies minerals, with implications for zircon geochronology in high-grade rocks. *Geology* 25, 607-610.
- [47]. Davidson, J., Turner, S., Handley, H., Macpherson, C., & Dosseto, A. (2007). Amphibole spong in arc crust?. *Geology*, 35, 787-790.
- [48]. Castillo, P.R. (2012). Adakite petrogenesis. *Lithos*, 134–135, 304–316.
- [49]. Castillo, P. R., Janney, P. E., & Solidum, R. U. (1999). Petrology and geochemistry of Camiguin Island, southern Philippines: insights to the source of adakites and other lavas in a complex arc setting. *Contributions to Mineralogy and Petrology*, 134, 33-51.

- [50]. Defant, M. J., & Kepezhinskas, P. (2001). Evidence suggests slab melting in arc magmas. *Eos, Transactions American Geophysical Union*, 82(6), 65-69.
- [51]. Drummond, M. S., Defant, M. J. & Kepezhinkas, P. K. (1996). Petrogenesis of slab-derived trondhjemite-tonalite-dacite/adakite magmas. Transactions of the Royal Society of Edinburgh: *Earth Sciences*, 87(1-2), 205-215.
- [52]. Martin, H. (1999). Adakitic magmas: modern analogues of Archaean granitoids. *Lithos*, 46(3), 411-429.
- [53]. Martin, H., Smithies, R. H., Rapp, R., Moyen, J. F., & Champion, D. (2005). An overview of adakite, tonalite-trondhjemite-granodiorite (TTG), and sanukitoid: relationships and some implications for crustal evolution. *Lithos*, 79, 1-24.
- [54]. Richards, J. P., & Kerrich, R. (2007). Special paper: adakite-like rocks: their diverse origins and questionable role in metallogenesis. *Economic geology*, 102(4), 537-576.
- [55]. Beate, B., Monzier, M., Spikings, R., Cotton, J., Silva, J., Bourdon, E., & Eissen, J. P. (2001). Mio-Pliocene adakite generation related to flat subduction in southern Ecuador: the Quimsacocha volcanic center. *Earth and Planetary Science Letters*, 192(4), 561-570.
- [56]. Smith, D. R., & Leeman, W. P. (1987). Petrogenesis of Mount St. Helens dacitic magmas. *Journal of Geophysical Research: Solid Earth*, 92(B10), 10313-10334.
- [57]. Azizi, H., & Moinevaziri, H. (2009). Review of the tectonic setting of Cretaceous to Quaternary volcanism in northwestern Iran. *Journal of Geodynamics*, 47(4), 167-179.
- [58]. Rapp, R.P., Watson, E.B., Miller, C.F. (1991). Partial melting of amphibolite/eclogite and the origin of Archean trondhjemites and tonalites. *Precambrian Research*, 51(1-4), 1-25.
- [59]. Wang, X. L., Shu, X. J., Xu, X., Tang, M., & Gaschnig, R. (2012). Petrogenesis of the Early Cretaceous adakite-like porphyries and associated basaltic andesites in the eastern Jiangnan orogen, southern China. *Journal of Asian Earth Sciences*, 61, 243-256.
- [60]. Breeding, C. M., Ague, J. J., & Bröcker, M. (2004). Fluid-metasedimentary rock interactions in subduction-zone mélanges: Implications for the chemical composition of arc magmas. *Geology*, 32(12), 1041-1044.
- [61]. Ma, Q., Zheng, J. P., Xu, Y. G., Griffin, W. L., & Zhang, R. S. (2015). Are continental "adakites" derived from thickened or foundered lower crust?, *Earth and Planetary Science Letters*, 419, 125-133.
- [62]. Dai, H.-K., Zheng, J., Zhou, X., Griffin, W.L. (2017). Generation of continental adakitic rocks: Crystallization modeling with variable bulk partition coefficients. *Lithos*, 272-273, 222-231.
- [63]. Deng, J., Yang, X., Qi, H., Zhang, Z. F., Mastoi, A. S. & Sun, W. (2017). Early Cretaceous high-Mg adakites associated with Cu-Au mineralization in the Cebu Island, Central Philippines: Implication for partial melting of the paleo-Pacific Plate. *Ore Geology Reviews*, 88, 251-269.
- [64]. Karsli, O., Dokuz, A., Uysal, İ., Aydin, F., Kandemir, R., & Wijbrans, J. (2010). Generation of the Early Cenozoic adakitic volcanism by partial melting of mafic lower crust, Eastern Turkey: implications for crustal thickening to delamination. *Lithos*, 114, 109-120.
- [65]. Kolb, J., Dziggel, A., & Schlatter, D. M. (2013). Gold occurrences of the Archean North Atlantic craton, southwestern Greenland: a comprehensive genetic model. *Ore Geology Reviews*, 54, 29-58.
- [66]. Wang, Q., Wyman, D. A., Xu, J. F., Zhao, Z. H., Jian, P., Xiong, X. L., & Bai, Z. H. (2006). Petrogenesis of Cretaceous adakitic and shoshonitic igneous rocks in the Luzong area, Anhui Province (eastern China): implications for geodynamics and Cu-Au mineralization. *Lithos*, 89(3-4), 424-446.
- [67]. Zhou, R. J., Chen, G. X., Li, Y., Zhou, C. H., Gong, Y., He, Y. L., & Li, X. G. (2005). Research on active faults in Litang-Batang region, Western Sichuan province, and the seismogenic structures of the 1989 Batang M6.7 earthquake swarm. *Seismol. Geol.* 1 (01), 31-43.
- [68]. Wang, Q., Xu, J. F., Jian, P., Bao, Z. W., Zhao, Z. H., Li, C. F., Xiong X. L., & Ma, J. L. (2006). Petrogenesis of adakitic porphyries in an extensional tectonic setting, Dexing, south China: Implications for the genesis of porphyry copper mineralization. *Journal of Petrology*, 47(1), 119-144.
- [69]. Arculus, R. J. (2003). Use and abuse of the terms calcalkaline and calcalkalic. *Journal of petrology*, 44(5), 929-935.
- [70]. Münker, C., Wörner, G., Yogodzinski, G., & Churikova, T. (2004). Behaviour of high field strength elements in subduction zones: Constraints from Kamchatka-Aleutian arc lavas. *Earth and Planetary Science Letters*, 224, 275-293.
- [71]. Ding, X., Lundstrom, C., Huang, F., Li, J., Zhang, Z. M., Sun, X. M., Liang, J. L., & Sun, W. D. (2009). Natural and experimental constraints on formation of the continental crust based on niobium-tantalum fractionation. *International Geology Review*, 51(6), 473-501.
- [72]. Foley, S., Tiepolo, M., & Vannucci, R. (2002). Growth of early continental crust controlled by melting

of amphibolite in subduction zones: *Nature*, 417, 837–840.

[73]. Moyen, J. F. (2009). High Sr/Y and La/Yb ratios: the meaning of the “adakitic signature”. *Lithos*, 112, 556-574.

[74]. Nagel, T. J., Hoffmann, J. E., & Münker, C. (2012). Generation of Eoarchean tonalitic-trondhjemitic-granodioritic from thickened mafic arc crust: *Geology*, 40, 375–378.

[75]. Hoffmann, J. E., Münker, C., Polat, A., Rosing, M. T., & Schulz, T. (2011). The origin of decoupled Hf-Nd isotope compositions in Eoarchean rocks from southern West Greenland. *Geochimica et Cosmochimica Acta*, 75, 6610-6628

[76]. Kay, S. M., & Mpodozis, C. (2001). Central Andean ore deposits linked to evolving shallow subduction systems and thickening crust. *GSA Today*, 11(3).

[77]. Gao, Y., Yang, Z., Santosh, M., Hou, Z., Wei, R., & Tian, S. (2010). Adakitic rocks from slab melt-modified mantle sources in the continental collision zone of southern Tibet. *Lithos*, 119(3-4), 651-663.

[78]. Wang, Q., Wyman, D. A., Zhao, Z. H., Xu, J. F., Bai, Z. H., Xiong, X. L., & Chu, Z. Y. (2007). Petrogenesis of Carboniferous adakites and Nb-enriched arc basalts in the Alataw area, northern Tianshan Range (western China): implications for Phanerozoic crustal growth in the Central Asia orogenic belt. *Chemical Geology*, 236(1-2), 42-64.

[79]. Zhang, Y. X., Tang, X. C., Zhang, K. J., Zeng, L., & Gao, C. L. (2014). U–Pb and Lu–Hf isotope systematics of detrital zircons from the Songpan–Ganzi Triassic flysch, NE Tibetan Plateau: Implications for provenance and crustal growth. *International Geology Review*, 56(1), 29-56.

[80]. Zhu, J. C., Wang, R. C., Zhang, P. H., Xie, C. F., Zhang, W. L., Zhao, K. D., Xie, L., Yang, C., Che, X. D., Yu, A., & Wang, L. B. (2009). Zircon U–Pb geochronological framework of Qitianling granite batholith, middle part of Nanling Range, South China. *Science in China Series D: Earth Sciences*, 52(9), 1279–1294.

[81]. Hou, Z. Q., Gao, Y. F., Qu, X. M., Rui, Z. Y., Mo, X. X. (2004). Origin of adakitic intrusives generated during mid-Miocene east–west extension in southern Tibet. *Earth and Planetary Science Letters*, 220(1-2): 139-155.

[82]. Zhao, X. B., Xue, C. J., Seltmann, R., Dolgoplova, A., Andersen, J. C. O., & Zhang, G. Z. (2020). Volcanic–plutonic connection and associated Au–Cu mineralization of the Tulasu ore district, Western Tianshan, NW China: Implications for mineralization potential in Palaeozoic arc terranes. *Geological Journal*, 55(3), 2318–2341.

[83]. O’Neill, H. S. C., & Palme, H., (1998). Composition of the silicate Earth: Implications for accretion and core formation. In: Jackson, I. (Ed.), *The Earth’s Mantle: Structure, Composition, and Evolution—The Ringwood Volume*. Cambridge University Press, Cambridge, 1, 3–126.

[84]. Yang, W. G., Zhong, Y., Zhu, L. D., Xie, L., Mai, Y. M., Li, N., Zhou, Y., Zhang, H. L., Xia, Tong, X., & Feng, W. N. (2022). The Early Cretaceous tectonic evolution of the Neo-Tethys: constraints from zircon U–Pb geochronology and geochemistry of the Liujiong adakite, Gongga, Tibet. *Geological Magazine*, 159(10), 1-16.

[85]. Ousta, S. h., Ashja-Ardalan, A., Yazdi, A., Dabiri, R., & Arian, M. A. (2024). Petrogenesis and tectonic implications of Miocene dikes in the southeast of Bam (SE Iran): Constraints on the development of active continental margin, *Geopersia*, 14 (1), 89-111. <https://doi.org/10.22059/geope.2023.364334.648729>

[86]. Guan, Q., Zhu, D. C., Zhao, Z. D., Dong, G. C., Zhang, L. L., Li, X. W., Liu, M., Mo, X. X., Liu, Y. S., & Yuan, H. L. (2012). Crustal thickening prior to 38 Ma in southern Tibet: evidence from lower crust-derived adakitic magmatism in the Gangdese Batholith. *Gondwana Research*, 21, 88-99.

[87]. Liu, J. N., Feng, C. Y., Qi, F., Li, G. C., Ma, S. C., & Xiao, Y. (2012). SIMS zircon U–Pb dating and fluid inclusion studies of Xiadeboli Cu–Mo ore district in Dulan County, Qinghai Province, *China Acta Petrology Sin* 28 (2), 679-690.

[88]. Wang Q, McDermott F, Xu J. f., Bellon, H., Zhu, Y.T. (2005). Cenozoic K-rich adakitic volcanic rocks in the Hohxil area, northern Tibet: lower-crustal melting in an intracontinental setting. *Geology*, 33(6), 465-468.

[89]. Hao, L. L., Wang, Q., Wyman, D. A., Ou, Q., Dan, W., Jiang, Z. Q., Wu, F. Y., Yang, J. H., Long, X. P., & Li, J. (2016). Underplating of basaltic magmas and crustal growth in a continental arc: evidence from Late Mesozoic intermediate–felsic intrusive rocks in southern Qiangtang, central Tibet. *Lithos*, 245, 223-242.

[90]. Ma, L., Wang, B. D., Jiang, Z. Q., Wang, Q., Li, Z. X., Wyman, D. A., Zhao, S. R., Yang, J. H., Gou, G. N., & Guo, H. F. (2014). Petrogenesis of the Early Eocene adakitic rocks in the Nagpuri area, southern Lhasa: partial melting of thickened lower crust during slab break-off and implications for crustal thickening in southern Tibet. *Lithos*, 196–197, 321–338.

[91]. Pang, K. N., Chung, S. L., Zarrinkoub, M. H., Li, X. H., Lee, H. Y., Lin, T. H., & Chiu, H. Y. (2016). New age and geochemical constraints on the origin of Quaternary adakite-like lavas in the Arabia-Eurasia collision zone. *Lithos*, 264, 348–359.

[92]. Baumann, A., Spies, O., & Lensch, G. (1983). Strontium isotopic composition of post ophiolitic Tertiary volcanics between kashmar, Sabzevar and

- Quchan/ NE Iran. Geodynamic project (Geotraverse) in Iran. *Geological Survey of Iran*. Report N 51.
- [93]. Spies, O., Lensch, G., & Mihm, A. (1983). Geochemistry of the post-ophiolitic Tertiary volcanic between Sabzevar and Quchan/NE-Iran. Geodynamic project (Geotraverse) in Iran. *Geological Survey of Iran*. Report N 51.
- [94]. Kay, R. W. (1978). Aleutian magnesian andesites: melts from subducted Pacific ocean crust. *Journal of Volcanology and Geothermal Research*, 4, 117-132.
- [95]. Rapp, R. P., Watson, E. B., & Miller, C. F. (1991). Partial melting of amphibolite/eclogite and the origin of Archean trondhjemites and tonalities. *Precambrian Research*, 51, 1-25.
- [96]. Zindler, A. & Hart, S. (1986). Chemical Geodynamics. *Annual Review of Earth and Planetary Sciences*, 14, 493-571.
- [97]. Defant, M. J., Jackson, T. E., Drummond, M. S., DeBoer, J. Z., Bellon, H., Feigenson, M. D., Maury, R. C., & Stewart, R. H. (1992). The geochemistry of young volcanism throughout western Panama and southeastern Costa Rica: an overview. *Journal of the Geological Society*, 149(4), 569-579.
- [98]. Asadi, S., Moore, F., & Zarasvandi, A. (2014). Discriminating productive and barren porphyry copper deposits in the southeastern part of the central Iranian volcano-plutonic belt, Kerman region, Iran: a review. *Earth-Science Reviews*, 138, 25-46.
- [99]. Ahmadian, J., Sarjoughian, F., Lentz, D., Esna-Ashari, A., & Murata, M. (2016). Eocene K-rich adakitic rocks in the Central Iran: Implications for evaluating its Cu–Au–Mo metallogenic potential. *Ore Geology*, 72, 323-342.
- [100]. Atherton, M. P., & Petford, N. (1993) Generation of sodium-rich magmas from newly underplated basaltic crust. *Nature*, 362, 144-146.
- [101]. Wang, H., Fu, B., Xu, Z., Lu, X., Lu, J., Li, H., Qu, W., Yang, X., Chen, W., & Zhang, J. (2015). Geology, geochemistry, and geochronology of the Wangjiazhuang porphyry–breccia Cu (–Mo) deposit in the Zouping volcanic basin, eastern North China Block. *Ore Geology Reviews*, 67, 336-353.
- [102]. Mousavi, S. Z., Darvishzadeh, A., Ghalamghash, J., Abedini, M. V. (2014). Volcanology and geochronology of Sabalan volcano, the highest stratovolcano in Azerbaijan region, NWIran. *Nautilus*, 128, 85-98.
- [103]. Maury, R. C., Sajona, F. G., Pubellier, M., Bellon, H., & Defant, M. J. (1996). Fusion de la croûte océanique dans les zones de subduction/collision récentes; l'exemple de Mindanao (Philippines). *Bulletin de la Société géologique de France*, 167(5), 579-595.
- [104]. Morris, P.A. (1995). Slab melting as an explanation of Quaternary volcanism and aseismicity in southwest Japan. *Geology*, 23(5), 395-398.
- [105]. Brophy, J. G., & Marsh, B. D. (1986). On the origin of high-alumina arc basalt and the mechanics of melt extraction: *Journal of Petrology*, 27(4), 763-789.
- [106]. Johnston, A. D. (1986). Anhydrous P-T phase relations of near-primary high-alumina basalt from the South Sandwich Islands: implications for the origin of island arcs and tonalite-trondhjemite. *Contrib Mineral Petrology*, 92, 368-382.
- [107]. Chung, S. L., Liu, D., Ji, J., Chu, M. F., Lee, H. Y., Wen, D. J., & Zhang, Q. (2003). Adakites from continental collision zones: melting of thickened lower crust beneath southern Tibet. *Geology*, 31(11), 1021-1024.
- [108]. Kay, R. W., & Kay, S. M. (1993). Delamination and delamination magmatism. *Tectonophysics*, 219, 177-189.
- [109]. Kay, R. W., & Kay, S. M. (2002). Andean adakites: three ways to make them. *Acta Petrologica Sinica*, 18(3), 303-311.
- [110]. Kay, S. M., Godoy, E., & Kurtz, A. (2005). Episodic arc migration, crustal thickening, subduction erosion, and magmatism in the south-central Andes. *Geological Society of America Bulletin*, 117(1-2), 67-88.
- [111]. Kay, S. M., Mpodozis, C., Ramos, V. A., Munizaga, F. (1991). Magma source variations for mid-late Tertiary magmatic rocks associated with a shallowing subduction zone and a thickening crust in the central Andes (28 to 33 S). *Geological Society of America Special Paper*, 265, 113-137.
- [112]. Yumul, G. P., Dimalanta, C., Bellon, H., Faustino, D. V., De Jesus, J. V., Tamayo, R. A., & Jumawan, F. T. (2000). Adakitic lavas in the Central Luzon back-arc region, Philippines: Lower crust partial melting products? *Island Arc*, 9(4), 499-512.
- [113]. Macpherson, C. G., Dreher, S. T., & Thirlwall, M. F. (2006). Adakites without slab melting: high pressure differentiation of island arc magma, Mindanao, the Philippines. *Earth and Planetary Science Letters*, 243(3-4), 581-593.
- [114]. Richards, J. R., & Kerrich, R. (2007). Adakite-like rocks: their diverse origins and questionable role in metallogenesis. *Economic Geology*, 102, 537-576.
- [115]. Rooney, T. O., Franceschi, P., & Hall, C. M. (2011). Water-saturated magmas in the Panama Canal region: a precursor to adakite-like magma generation? *Contributions to mineralogy and petrology*, 161(3), 373-388.
- [116]. Sell , D., Dungan, M., Langmuir, C., & Leeman, W. (2007). Adakitic Dacites Formed by Intracrustal Crystal Fractionation of Water-rich Parent Magmas at

- Nevado de Longavi Volcano (36 {middle dot} 2 {degrees} S; Andean Southern Volcanic Zone, Central Chile). *Journal of petrology*, 48(11).
- [117]. Hidalgo, P. J., & Rooney, T. O. (2010). Crystal fractionation processes at Baru volcano from the deep to shallow crust. *Geochemistry, Geophysics, Geosystems*, 11(12).
- [118]. Hidalgo, P.J., & Rooney, T.O. (2014). Petrogenesis of a voluminous Quaternary adakitic volcano: the case of Baru volcano. *Contributions to mineralogy and petrology*, 168(3), 1-19.
- [119]. Macpherson, C. G., Dreher, S. T., Thirlwall, M. F., (2006). Adakites without slab melting: high pressure differentiation of island arc magma, Mindanao, the Philippines. *Earth and Planetary Science Letter* 243, 581-593.
- [120]. Nakamura, H., & Iwamori, H. (2013). Generation of adakites in a cold subduction zone due to double subducting plates. *Contributions to mineralogy and petrology*, 165(6), 1107-1134.
- [121]. Jahangiri, A. (2007). Post-collisional Miocene adakitic volcanism in NW Iran: geochemical and geodynamic implications. *Journal of Asian Earth Sciences*, 30, 433-447.
- [122]. Amel ,N., Jalili Ghareh Ghaye, V., Hajjialioghli, R., & Moayyed, M. (2015). Petrogenesis of adakitic Plio-Quaternary post collision rocks, north of Sahand volcano (NW of Iran). *Iranian Journal of Petrology*, 6(22), 157-172.
- [123]. Moharami Gargari, F., Gorbani, M., & Pourmoafee, M. (2015). Geochemistry and petrogenesis of Adakitic rocks from the Kiyamaki magmatic dome, southeast Jolfa (NW Iran). *Iranian Society of crystallography and mineralogy*, 32, 2.
- [124]. Delavari, M., Amini, S., Schmitt, A. K., McKeegan, K. D., & Harrison, T. M. (2014). U–Pb geochronology and geochemistry of Bibi-Maryam pluton, eastern Iran: implication for the late stage of the tectonic evolution of the Sistan Ocean. *Lithos*, 200, 197-211.
- [125]. Topuz, G., Altherr, R., Schwarz, W. H., Siebel, W., Satir, M., & Dokuz, A. (2005). Post-collisional plutonism with adakite-like signatures: the Eocene Saraycik granodiorite (Eastern Pontides, Turkey). *Contributions to mineralogy and petrology*, 150(4), 441-455.
- [126]. Qian, Q., & Hermann, J. (2013). Partial melting of lower crust at 10–15 kbar: Constraints on adakite and TTG formation. *Contributions to Mineralogy and Petrology*, 165(6), 1195–1224.
- [127]. Zor, E. (2008). Tomographic evidence of slab detachment beneath eastern Turkey and the Caucasus. *Geophysical Journal International*, 175(3), 1273-1282.
- [128]. Maggi, A., & Priestley, K. (2005). Surface waveform tomography of the Turkish–Iranian plateau. *Geophysical Journal International*, 160(3), 1068-1080.
- [129]. Taghizadeh, F., Sodoudi, F., Afsari, N., & Ghassemi, M. R. (2010). Lithospheric structure of NW Iran from P and S receiver functions. *Journal of seismology*, 14(4), 823-836.
- [130]. Agard, P., Omrani, J., Jolivet, L., & Mouthereau, F. (2005). Convergence history across Zagros (Iran): constraints from collisional and earlier deformation. *International journal of earth sciences*, 94(3), 401-419.
- [131]. Agard, P., Omrani, J., Jolivet, L., Whitechurch, H., Vrielynck, B., Spakman, & Wortel, R. (2011). Zagros orogeny: a subduction-dominated process. *Geological Magazine*, 148(5-6), 692-725.
- [132]. Madanipour, S., Ehlers, T. A., Yassaghi, A., Enkelmann, E. (2017). Accelerated middle Miocene exhumation of the Talesh Mountains constrained by U-Th/He thermochronometry: Evidence for the Arabia-Eurasia collision in the NW Iranian Plateau. *Tectonics*, 36(8), 1538-1561.
- [133]. Lechmann, A., Burg, J.P., Ulmer, P., Guillong, M., & Faridi, M. (2018). Metasomatized mantle as the source of Mid-Miocene-Quaternary volcanism in NW-Iranian Azerbaijan: Geochronological and geochemical evidence. *Lithos*, 304, 311-328.
- [134]. Pearce, J. A., Bender, J., De Long, S., Kidd, W., Low, P., Güner, Y., & Mitchell, J. (1990). Genesis of collision volcanism in Eastern Anatolia, Turkey. *Journal of Volcanology and Geothermal Research*, 44(1-2), 189-229.
- [135]. Moghadam, H.S., Corfu, F., Chiaradia, M., Stern, R. J., & Ghorbani, G. (2014). Sabzevar Ophiolite, NE Iran: Progress from embryonic oceanic lithosphere into magmatic arc constrained by new isotopic and geochemical data. *Lithos*, 210, 224-241.
- [136]. Aftabi, A., & Atapour, H. (2000). Regional aspects of shoshonitic volcanism in Iran. *Episodes*, 23(2), 119-125.
- [137]. Fazlnia, A. (2019). Origin and magmatic evolution of the Quaternary syn-collision alkali basalts and related rocks from Salmas, northwestern Iran. *Lithos*, 344, 297-310.
- [138]. Yener Eyuboglu, A.M., Santosh, B.C., Keewook, Yi, D., Osman Bektaş, A., & Sanghoon, K. (2012). Discovery of Miocene adakitic dacite from the Eastern Pontides Belt (NE Turkey) and a revised geodynamic model for the late Cenozoic evolution of the Eastern Mediterranean region. *Lithos*, 146–147: 218-232.
- [139]. Hempton, M. R. (1987). Constraints on Arabian plate motion and extensional history of the Red Sea. *Tectonics*, 6(6): 687-705.
- [140]. Karim, K. H., Koyi, H., Baziany, M. M., & Hessami, K. (2011). Significance of angular

unconformities between Cretaceous and Tertiary strata in the northwestern segment of the Zagros fold-thrust belt, Kurdistan Region, NE Iraq. *Geological Magazine*, 148(5-6), 925-939.

[141]. McQuarrie, N., Stock, J., Verdel, C., & Wernicke, B. (2003). Cenozoic evolution of Neotethys and implications for the causes of plate motions. *Geophysical research letters*, 30(20).

[142]. Vincent, S. J., Allen, M. B., Ismailzadeh, A. D., Flecker, R., Foland, K. A., & Simmons, M. D. (2005). Insights from the Talysh of Azerbaijan into the Paleogene evolution of the South Caspian region. *Geological Society of America Bulletin*, 117(11-12), 1513-1533.

[143]. Seyedrahimi-Niaraq, M., Bina, S. M., Itoi, R. (2021). Numerical and thermodynamic modeling for estimating production capacity of NW Sabalan geothermal field, Iran. *Geothermics*, 90.

[144]. Seyedrahimi-Niaraq, M., Doulati Ardejani, F., Noorollah, Y., & Porkhial, S. (2017). Development of an updated geothermal reservoir conceptual model for NW Sabalan geothermal field, Iran. *Geotherm Energy*, 5, 14.

[145] Seyedrahimi-Niaraq, M., Doulati Ardejani, F., Noorollah, Y., Nasrabadi, S. J., & Hekmatnejad, A. (2021). An unsaturated three-dimensional model of fluid flow and heat transfer in NW Sabalan geothermal reservoir. *Geothermics*, 89.

[146]. Berberian, F., & Berberian, M. (1981). Tectono-plutonic episodes in Iran. *Zagros Hindu Kush Himalaya Geodynamic Evolution*, 3, 5-32.

[147]. Keskin, M., Pearce, J. A., Kempton, P. D., & Greenwood, P. (2006). Magma-crust interactions and magma plumbing in a postcollisional setting: geochemical evidence from the Erzurum-Kars volcanic plateau, eastern Turkey. *Special papers-geological society of america*, 409, 475.

[148]. Djamour, M. Y., Vernant, P., Nankali, H. R., Tavakoli, F. (2011). NW Iran-eastern Turkey present-day kinematics: results from the Iranian permanent GPS network. *Earth and Planetary Science Letters*, 307(1-2), 27-34.

[149]. Fedele, Z., Mehdipour Ghazi, J., Agostini, S., Ronca, S., Innocenzi, F., & Lustrino, M. (2023). Concurrent adakitic and non-adakitic Late Miocene-Quaternary magmatism at the Sahand volcano, Urumieh-Dokhtar Magmatic Arc (NW Iran). *Lithos*, 458-459, 107344.

[150]. Nazari, M., Arian, M. A., Solgi, A., Zareisahamieh, R., & Yazdi, A. (2023). Geochemistry and tectonomagmatic environment of Eocene volcanic rocks in the Southeastern region of Abhar, NW Iran, *Iranian Journal of Earth Sciences*, 15(4), 228-247. <https://doi.org/10.30495/ijes.2023.1956689.1746>

[151]. Moghimi, H., Rezaeian, M., & Sobouti, F. (2016). Analysis of Structural Fractures in Sabalan Volcano. *Master's Structural s Thesis*, 156.

رخداد آداکیت پلیو-کواترنری و فرآیندهای پس از برخورد: شیمی سنگ کل و ترکیبات ایزوتوپی استرانسیم-نئودیمیم، در کمر بند ماگمایی البرز، اردبیل، ایران

اکرم عبدالاحدی^۱، سید جمال شیخ ذکریایی^۱، عبدالله یزدی^{۲*} و سید زاهد موسوی^۳

۱- گروه زمین شناسی، واحد علوم و تحقیقات، دانشگاه آزاد اسلامی، تهران، ایران

۲- گروه زمین شناسی، واحد کهنوج، دانشگاه آزاد اسلامی، کهنوج، ایران

۳- گروه زمین شناسی، واحد مشکین شهر، دانشگاه آزاد اسلامی، مشکین شهر، ایران

ارسال ۲۰۲۴/۰۷/۱۳، پذیرش ۲۰۲۴/۱۰/۲۱

* نویسنده مسئول مکاتبات: yazdi_mt@yahoo.com

چکیده:

گنبد‌های ساب ولکانیک پلیو-کواترنری محصول ماگماتیسیم در فلات ترکیه-ایران در منطقه برخورد بین اوراسیا و عربستان هستند. در ۵۰ کیلومتری غرب اردبیل سنگ‌های آتشفشانی فلسیک میانی یافت می‌شود. این گنبد‌های آتشفشانی بخش مهمی از آتشفشان سبلان، یک آتشفشان چین‌های پلیو-کواترنری در شمال غربی ایران را تشکیل می‌دهند. سنگ‌های آذرین (آداکیت) شامل داسیت، تراکیت، آندزیت، تراکی آندزیت و تراکی داسیت هستند که همراه با اینگیمبریت و سنگ‌های آذرآواری در منطقه مشاهده می‌شوند. آنها عمدتاً شامل فنوکریست‌ها و ریز بلورهای از پیروکسن، آمفیبول و پلاژیوکلاز با بیوتیت و تیتانومگنتیت هستند. این سنگ‌ها با عناصر کمیاب خاکی سبک (LRREs) و عناصر لیتوفیل بزرگ یون (LILEs) غنی شده و از عناصر خاکی کمیاب سنگین (HRREs) و عناصر قدرت میدان بالا (HFSEs) تهی شده‌اند. در این سنگ‌ها، محتوای SiO_2 (56-66) وزنی، $\text{Na}_2\text{O} > 3.5$ وزنی، $\text{Al}_2\text{O}_3 > 15$ وزنی، $\text{Yb} < 0.2$ ppm و $Y < 7$ ppm است که شاخص سنگ‌های آداکیت سیلیس بالا است. نسبت‌های اولیه $^{143}\text{Nd}/^{144}\text{Nd}$ از ۰/۵۱۲۷ تا ۰/۵۱۲۹ و نسبت‌های اولیه $^{86}\text{Sr}/^{87}\text{Sr}$ برای آداکیت‌ها از ۰/۷۰۳۵ تا ۰/۷۰۶۰ متغییر است که منعکس کننده ناهمگنی گوشته و درجات مختلف ذوب است. این داده‌های زمین‌شناسی، ژئوشیمیایی و ایزوتوپی استرانسیم و نئودیمیم نشان می‌دهد که این سنگ‌ها متعلق به نوع آداکیت پس از برخورد هستند و نشان دهنده اشتقاق ماگمای آنها از ذوب بخشی درجه پائین یک گوشته لیتوسفری قاره‌ای که توسط ورقه فرورانش شده دچار متاسوماتیزم شده است، می‌باشد. در منطقه مورد مطالعه کانی‌سازی مربوط به سنگ‌های آداکیتی پلیو-کواترنری مشاهده نشده است.

کلمات کلیدی: کمر بند ماگمایی البرز، ایزوتوپ Sr-Nd، آداکیت، سبلان، ایران.